UNIVERSITY OF PATRAS

DEPARTMENT OF ELECTRICAL AND COMPUTER ENGINEERING

DIVISION OF TELECOMMUNICATIONS & INFORMATION TECHNOLOGY
WIRE COMMUNICATIONS LABORATORY
VISUALIZATION & VIRTUAL REALITY GROUP

Multiphase dynamic simulation for realistic reconstruction of volcanic activity on Santorini, Greece

D I P L O M A T H E S I S

KONSTANTINOS GAVALAS

SUPERVISOR: KONSTANTINOS MOUSTAKAS

PATRAS – JUNE 2024

University of Patras, Department of Electrical and Computer Engineering.

Konstantinos Gavalas

© 2024 – All rights reserved

The whole work is an original work, produced by Konstantinos Gavalas, and does not violate the rights of third parties in any way. If the work contains material which has not been produced by him, this is clearly visible and is explicitly mentioned in the text of the work as a product of a third party, noting in a similarly clear way his identification data, while at the same time confirming that in case of using original graphics representations, images, graphs, etc., has obtained the unrestricted permission of the copyright holder for the inclusion and subsequent publication of this material.

CERTIFICATION

It is certified that the Diploma Thesis titled

Multiphase dynamic simulation for realistic reconstruction of volcanic activity on Santorini, Greece

of the Department of Electrical and Computer Engineering student

KONSTANTINOS GAVALAS

Registration Number: 1072772

was presented publicly at the Department of Electrical and Computer Engineering at

2024 - 06 - 27

and was examined by the following examining committee:

Konstantinos Moustakas, Associate Professor, Department of Electrical and Computer Engineering (supervisor)

Kyriakos Sgarbas, Associate Professor, Department of Electrical and Computer Engineering (committee member)

Pavlos Peppas, Professor, Department of Electrical and Computer Engineering (committee member)

The Supervisor	The Director of the Division
Konstantinos Moustakas Associate Professor	Logothetis Michael Professor

ΠΑΝΕΠΙΣΤΗΜΙΟ ΠΑΤΡΩΝ
ΤΜΗΜΑ ΗΛΕΚΤΡΟΛΟΓΩΝ ΜΗΧΑΝΙΚΩΝ ΚΑΙ ΤΕΧΝΟΛΟΓΙΑΣ ΥΠΟΛΟΓΙΣΤΩΝ

ΤΟΜΕΑΣ ΤΗΛΕΠΙΚΟΙΝΩΝΙΩΝ ΚΑΙ ΤΕΧΝΟΛΟΓΙΑΣ ΠΛΗΡΟΦΟΡΙΑΣ
ΕΡΓΑΣΤΗΡΙΟ ΕΝΣΥΡΜΑΤΗΣ ΤΗΛΕΠΙΚΟΙΝΩΝΙΑΣ & ΤΕΧΝΟΛΟΓΙΑΣ ΤΗΣ ΠΛΗΡΟΦΟΡΙΑΣ
ΟΜΑΔΑ ΑΠΕΙΚΟΝΙΣΗΣ ΠΛΗΡΟΦΟΡΙΑΣ ΚΑΙ ΕΙΚΟΝΙΚΗΣ ΠΡΑΓΜΑΤΙΚΟΤΗΤΑΣ

Δυναμική προσομοίωση πολλαπλών φάσεων για ρεαλιστική αναπαράσταση ηφαιστειακής δραστηριότητας στη Σαντορίνη

Δ Ι Π Λ Ω Μ Α Τ Ι Κ Η Ε Ρ Γ Α Σ Ι Α

ΚΩΝΣΤΑΝΤΙΝΟΣ ΓΑΒΑΛΑΣ

ΕΠΙΒΛΕΠΩΝ: ΚΩΝΣΤΑΝΤΙΝΟΣ ΜΟΥΣΤΑΚΑΣ

ΠΑΤΡΑ - ΙΟΥΝΙΟΣ 2024

Πανεπιστήμιο Πατρών, Τμήμα Ηλεκτρολόγων Μηχανικών και Τεχνολογίας Υπολογιστών.

Κωνσταντίνος Γαβαλάς

© 2024 – Με την επιφύλαξη παντός δικαιώματος

Το σύνολο της εργασίας αποτελεί πρωτότυπο έργο, παραχθέν από τον Κωνσταντίνο Γαβαλά, και δεν παραβιάζει δικαιώματα τρίτων καθ' οποιονδήποτε τρόπο. Αν η εργασία περιέχει υλικό, το οποίο δεν έχει παραχθεί από τον ίδιο, αυτό είναι ευδιάκριτο και αναφέρεται ρητώς εντός του κειμένου της εργασίας ως προϊόν εργασίας τρίτου, σημειώνοντας με παρομοίως σαφή τρόπο τα στοιχεία τακτοποίησής του, ενώ παράλληλα βεβαιώνει πως στην περίπτωση χρήσης αυτούσιων γραφικών αναπαραστάσεων, εικόνων, γραφημάτων κ.λπ., έχει λάβει τη χωρίς περιορισμούς άδεια του κατόχου των πνευματικών δικαιωμάτων για τη συμπερίληψη και επακόλουθη δημοσίευση του υλικού αυτού.

ΠΙΣΤΟΠΟΙΗΣΗ

Πιστοποιείται ότι η Διπλωματική Εργασία με τίτλο

Δυναμική προσομοίωση πολλαπλών φάσεων για ρεαλιστική αναπαράσταση ηφαιστειακής δραστηριότητας στη Σαντορίνη

του φοιτητή του Τμήματος Ηλεκτρολόγων Μηχανικών και Τεχνολογίας Υπολογιστών

ΚΩΝΣΤΑΝΤΙΝΟΥ ΓΑΒΑΛΑ ΤΟΥ **ΕΥΑΓΓΕΛΟΥ**

Αριθμός Μητρώου: 1072772

Παρουσιάστηκε δημόσια στο Τμήμα Ηλεκτρολόγων Μηχανικών και Τεχνολογίας Υπολογιστών στις

2024 - 06 - 27

και εξετάστηκε από την ακόλουθη εξεταστική επιτροπή:

Κωνσταντίνος Μουστάκας, Αναπληρωτής Καθηγητής, Τμήμα Ηλεκτρολόγων Μηχανικών και Τεχνολογίας Υπολογιστών (επιβλέπων)

Κυριάκος Σγάρμπας, Αναπληρωτής Καθηγητής, Τμήμα Ηλεκτρολόγων Μηχανικών και Τεχνολογίας Υπολογιστών (μέλος επιτροπής)

Παύλος Πέππας, Καθηγητής, Τμήμα Ηλεκτρολόγων Μηχανικών και Τεχνολογίας Υπολογιστών
(μέλος επιτροπής)

Ο Επιβλέπων	Ο Διευθυντής του Τομέα
Κωνσταντίνος Μουστάκας	Μιχαήλ Λογοθέτης
Αναπληρωτής Καθηγητής	Καθηγητής

ACKNOWLEDGEMENTS

I would like to start by expressing my deepest gratitude to my supervisor, Dr. Konstantinos Moustakas, for his unwavering support and guidance throughout this project. His mentorship, which began well before this year-long journey, and his encouragement to pursue ambitious and unconventional ideas have significantly contributed to my development as an engineer and as an individual.

I am also immensely grateful for the expertise and support provided by Dr. Paraskevi V. Nomikou, whose enthusiasm and geological insights profoundly influenced my approach and greatly enhanced the quality of this work.

Furthermore, I would like to extend my heartfelt thanks to my family and friends for their continuous support and encouragement. Their belief in me has been a constant source of motivation and strength throughout my academic pursuits and in all aspects of my life.

Finally, I must also acknowledge the pivotal role of the entire open source community in providing the tools essential for the success of this work. In no particular order I'd specifically like to mention *Manjaro Linux* for their stability as an operating system throughout this project, *Blender* for freely providing some of the best tools in 3D graphics, *Inkscape* for helping me create all the figures in this work, and *TeXstudio* for facilitating the preparation of this text in LaTeX.

ABSTRACT

Multiphase dynamic simulation for realistic reconstruction of volcanic activity on Santorini, Greece

Konstantinos Gavalas **Konstantinos Moustakas**

This work explores the potential applications of computer graphics techniques for the realistic visualization of volcanic events, with the ultimate goal of augmenting science communication efforts. The 1650 CE eruption of Kolumbo in Santorini, Greece is used as a case study to highlight the strengths and weaknesses of different visualization methods for a variety of complex phenomena. Presented first is the 3D reconstruction of the island and seabed based on satellite and bathymetry data, using an automated tool specifically developed for this goal. Then, several subaerial phenomena are examined, with the most notable results yielded by the volcanic plume simulations. Next, shifting focus to the submarine phenomena and especially the catastrophic tsunamogenic collapse of the northwest flank of the volcanic cone, the use of a modified version of the mass-spring model for the simulation of soft bodies is presented. Finally, despite these promising results, several limitations of the available tools and techniques observed in this interdisciplinary context are also discussed.

ΕΚΤΕΤΑΜΕΝΗ ΕΛΛΗΝΙΚΗ ΠΕΡΙΛΗΨΗ

Δυναμική προσομοίωση πολλαπλών φάσεων για ρεαλιστική αναπαράσταση ηφαιστειακής δραστηριότητας στη Σαντορίνη

Κωνσταντίνος Γαβαλάς **Κωνσταντίνος Μουστάκας**

Καθώς βελτιώνεται η επιστημονική κατανόηση των μηχανισμών που διέπουν τα διάφορα φυσικά φαινόμενα που μας περιβάλλουν, ιδιαίτερο ενδιαφέρον δημιουργείται στην ανάπτυξη νέων τρόπων επικοινωνίας των ευρημάτων αυτών τόσο προς το ευρύτερο κοινό, όσο και προς τις αρμόδιες αρχές. Η αξιοποίηση τεχνικών από την επιστήμη των γραφικών υπολογιστών για τη ρεαλιστική απεικόνιση των φαινομένων, θα μπορούσε να διαδραματίσει πρωταγωνιστικό ρόλο στις προσπάθειες αυτές.

Συγκεκριμένα, στα πλαίσια της παρούσας διπλωματικής εργασίας, εξετάζεται η εφαρμογή των τεχνικών αυτών στον τομέα της ηφαιστειολογίας. Ως παράδειγμα, η εργασία επικεντρώνεται στην ηφαιστειακή έκρηξη του 1650 στο Κολούμπο της Σαντορίνης, όπου πρόσφατες επιστημονικές ανακαλύψεις, σε συνδυασμό με υπάρχουσες ιστορικές αναφορές, μας παρέχουν μια σαφή εικόνα των ποικιλόμορφων φαινομένων.

Παρουσιάζεται αρχικά η απαιτούμενη διαδικασία για τη ρεαλιστική τρισδιάστατη απεικόνιση του νησιού της Σαντορίνης και του βυθού, βάση δορυφορικών δεδομένων και δεδομένων βαθυμετρίας. Για τον σκοπό αυτό, αναπτύσσεται επιπλέον και ένα εξειδικευμένο, αυτοματοποιημένο εργαλείο. Τα παραγόμενα μοντέλα διατηρούν την πραγματική κλίμακα της τοπολογίας και μας επιτρέπουν τη δημιουργία ενός ακριβούς εικονικού περιβάλλοντος.

Στη συνέχεια, ξεκινώντας από τα φαινόμενα που μαίνονται πάνω από την επιφάνεια της θάλασσας, σημαντικά αποτελέσματα επιτυγχάνονται στην απεικόνιση ηφαιστειακών νεφών με χρήση μίας υβριδικής μεθόδου βασισμένης σε τεχνικές προσομοίωσης σωματιδίων. Περιγράφονται επίσης συνοπτικά τεχνικές για την οπτικοποίηση ηφαιστειακών τσουνάμι, σεισμών και κεραυνών.

Περνώντας στα υποθαλάσσια φαινόμενα, βασικό σημείο ενδιαφέροντος αποτελεί η κατάρρευση της βορειοδυτικής πλευράς του σχηματισμένου ηφαιστειακού κώνου. Για την απεικόνιση του φαινομένου αυτού, παρουσιάζεται μια τεχνική προσομοίωσης μαλακών σωμάτων βασισμένη σε μια τροποποιημένη εκδοχή του μοντέλου μάζας-ελατηρίου. Περιγράφονται επίσης τεχνικές για την οπτικοποίηση της διαδικασίας δημιουργίας του ηφαιστειακού κώνου.

Τέλος, παρά τα ενθαρρυντικά αποτελέσματα αυτά, γίνεται αναφορά και στους περιορισμούς των διαθέσιμων εργαλείων και τεχνικών που προκύπτουν από τον διεπιστημονικό χαρακτήρα της εργασίας.

Contents

1 Introduction **12**
1.1 Significance of Realistic Visualizations in Geoscience 12
1.2 Santorini's Volcanic Activity 12
1.2.1 General Background 12
1.2.2 The 1650 CE Eruption of Kolumbo 13
1.3 Modern Simulation and Visualization Techniques 16
1.3.1 General Workflow 16
1.3.2 Computational Physics 16
1.3.3 Applications in Geoscience 18

2 Island and Seabed Reconstruction **20**
2.1 Digital Elevation Models and Heightmaps 20
2.2 Conversion to Usable 3D Models 21
2.2.1 Basic Methodology and Complications 21
2.2.2 hm2obj: Automatic Conversion 22
2.2.3 Results 22
2.3 Realistic Rendering 23
2.3.1 Procedural Textures in Blender 23
2.3.2 Realistic Materials and Illumination 24
2.3.3 Results 25

3 Subaerial Phenomena **26**
3.1 Volcanic Plume and Smoke Simulations 26
3.2 Tsunami Simulation and Visualization 29
3.3 Secondary Phenomena 30

4 Submarine Phenomena **31**
4.1 Seabed and Hydrothermal Vents 31
4.2 Cone Formation 32
4.3 Flank Collapse 33
4.3.1 Volcanic Cone Model 34
4.3.2 Simulating Using Existing Tools 36
4.3.3 Use of Rigid Body Physics for Mesh Deformation 37
4.3.4 Results 41

5 Discussion and Conclusion **45**
5.1 Overview of Results 45
5.2 Limitations 46
5.3 Future Directions 47
5.4 Final Thoughts 47

Acronyms

API Application Programming Interface. 36, 37

BCE Before Common Era. 12
BSDF Bidirectional Scattering Distribution Function. 24, 42

CE Common Era. 10, 13–16, 19–23, 25, 26, 28–33, 45, 47
CFD Computational Fluid Dynamics. 17
CG Computer Graphics. 12, 13, 15–18, 20, 26–28, 30, 32, 34, 36, 39, 46, 47
CPU Central Processing Unit. 16, 27

DEM Digital Elevation Model. 20, 45
DNS Direct Numerical Simulation. 17

FEM Finite Element Method. 18, 34
FVM Finite Volume Method. 19

GIS Geographic Information System. 18, 20, 46
GPS Global Positioning System. 18
GPU Graphics Processing Unit. 16, 17, 27
GUI Graphical User Interface. 36, 47

HTHH Hunga Tonga–Hunga Ha'apai. 19, 26, 28, 30

IOR Index of Refraction. 24

LBA Late Bronze Age. 12, 13
LOD Level of Detail. 20

ML Machine Learning. 17, 47
MR Mixed Reality. 19
MSM Mass-Spring Model. 18, 36, 37, 39, 43, 45, 47

OBB Oriented Bounding Box. 17

PDE Partial Differential Equation. 16, 18

ROV Remotely Operated Vehicle. 31

SPH Smoothed Particle Hydrodynamics. 18

TPU Tensor Processing Unit. 17

UAV Unmanned Aerial Vehicle. 29

VR Virtual Reality. 18–20

1 Introduction

1.1 Significance of Realistic Visualizations in Geoscience

Science Communication

With critique of science and technology growing over the past decades, *science communication* has become a crucial profession and field of study [1]. Computer-generated media has lead to a lot of controversy in recent years [2], [3], but the use of modern Computer Graphics (CG) by science communicators for the creation of realistic visualizations could greatly benefit the public, making knowledge more approachable and easy to understand for all.

Realistic Visualizations

Visualizations have been shown to affect hurricane risk assessment [4], improve expert and public understanding of weather forecasts [5], and generally enhance critical thinking of students [6]. Modern visualization techniques are not limited to comprehensive graphs and plots. The field of CG has seen major development since its inception in the early 1950s [7] allowing for improved realism, especially in non-real-time applications. Images generated using modern CG techniques are indistinguishable from ones produced by real-world digital photography, even by professional photographers and editors [8].

In the context of Geoscience, raising awareness of natural hazards and communicating risk to citizens is considered a top priority [9]. This is a perfect application for realistic CG visualizations, as the danger of most geological hazards (e.g. volcanoes) cannot be easily imagined or understood without true-to-life visual aids. The Kolumbo submarine volcano in Santorini, Greece for example, is currently not viewed as a threat by decision makers even though it is considered the most dangerous active volcano in the Mediterranean by scientists working in the field [10].

1.2 Santorini's Volcanic Activity

1.2.1 General Background

The Island of Santorini

Santorini, also known as Thira, is a Greek island laying on top of the South Aegean Volcanic Arc. Based on a 2021 census, the island has a population of 15 457, with that number expanding to over 500 000 during the peak of the summer tourism period [10], [11]. The island is mostly known for its unique landscape, with most of the attention falling on the vast water-filled west-facing caldera. The steep caldera cliffs were created after one of the most violent volcanic eruptions in human history, known as the Late Bronze Age (LBA) eruption, which took place between 1627 BCE and 1500 BCE (~3.6 ka) [12]. The eruption caused about half of the original island (see Fig. 1) to sink into the sea and generated a tsunami with a run-up of at least 9 meters that reached the present-day island of Crete, the coast of Turkey as well as Israel [12].

Eruptive Centers

Contrary to popular belief, the eruptive centers of Santorini are not all located within the present-day caldera. Although both the LBA eruption and all recent eruptive activity has been contained in this area, multiple other eruptive centers also exist outside the boundaries of the island. As seen on Fig. 2, these centers are located atop a northeast-trending line, with the most prominent outside the caldera being the Christiana islands and Kolumbo [13]. In recent years, the Kolumbo eruptive center has become a notable point of interest and concern for scientists.

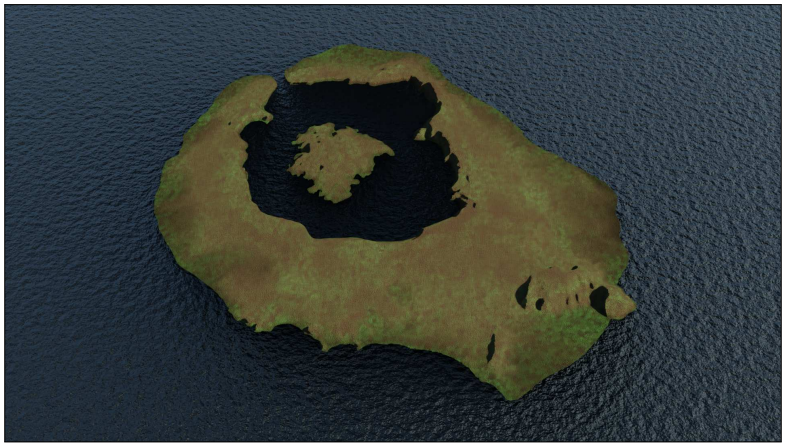

Fig. 1. The island that stood in place of modern-day Santorini before the LBA eruption, also known as Strogili (CG render based on the findings of [14])

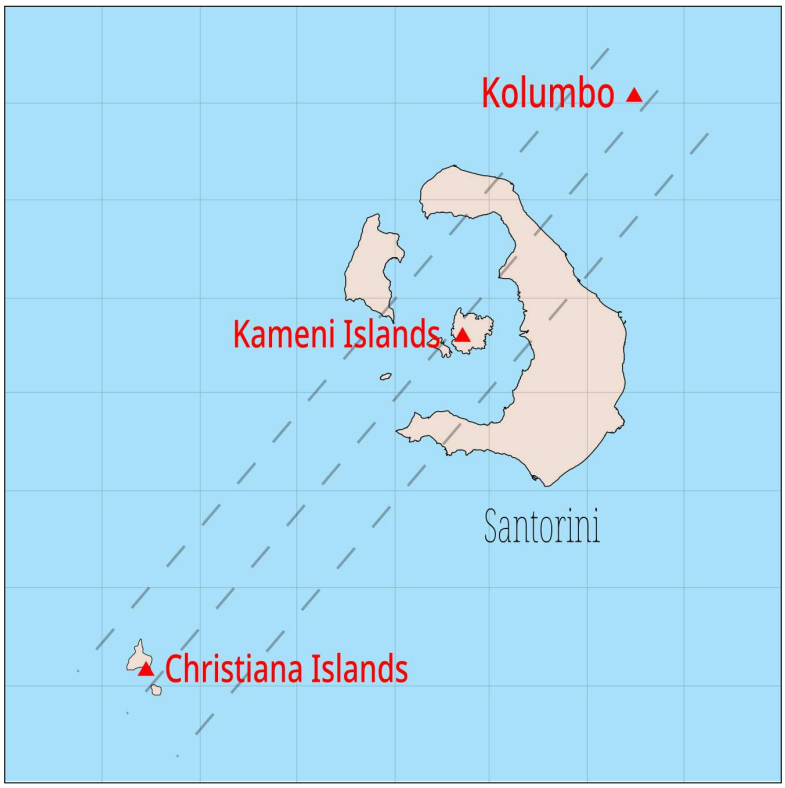

Fig. 2. A map of Santorini and its eruptive centers (marked by red triangles)

1.2.2 The 1650 CE Eruption of Kolumbo

Kolumbo Submarine Volcano

The Kolumbo submarine volcano, part of the Kolumbo volcanic field, is located 7 kilometers off the northeastern coast of Santorini (see Fig. 2) and is mostly known for a major eruption in 1650 CE. Bathymetric maps of the area [15], [16] show a stunning crater and submarine caldera. The crater extends 2500 meters wide, with its shallowest point at a depth of 18m in the south-west and its deepest at 500m below sea level (see Fig. 3).

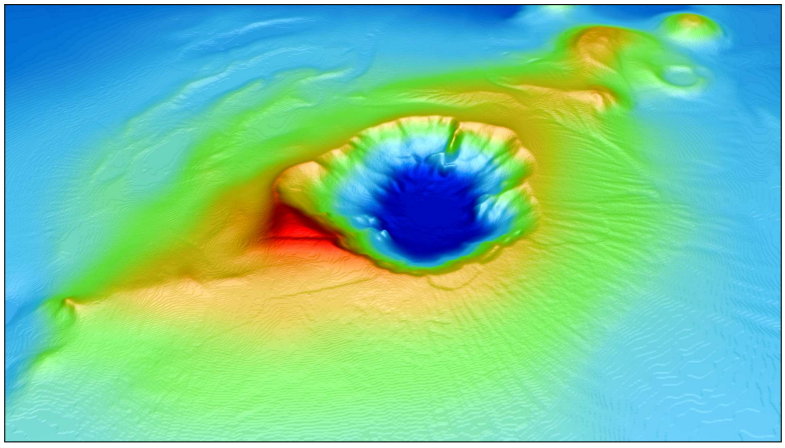

Fig. 3. 3D reconstruction of the Kolumbo crater as seen from the south based on bathymetry data

1650 CE Eruption

Being the largest eruption in Santorini in historic years, the Kolumbo eruption of 1650 CE provides a unique opportunity to study the hazards of a submarine volcanic eruption not only using in-situ deposits of volcanic material but also taking into account first-hand witness statements [17]. A timeline of events, as well as all available testimonies from that period was first compiled by french geologist Ferdinard A. Fouqué in 1879 [18]. Combined with recent research efforts [19], these historic accounts allow us for a very accurate recreation of the events that took place around the time of the eruption.

Before 1650 CE no eruption, or other volcanic activity, has struck the island since 1573 CE. The main island has the same shape as today, with the only difference being that a smaller island, known as Mikra Kameni, exists in place of today's Nea Kameni within the caldera (see Fig. 4) [20]. Starting in 1649 CE and peaking on the 27th of September 1650 CE intense seismic activity shakes the island. After these violent earthquakes, the inhabitants start noticing smoke and flames rising from within the sea northeast of Santorini. They also note a strong noxious odor that soon spreads across the entire island. From within the smoke, they detect a small snow-white island that has formed in that area.

Columns of smoke rise and quickly disappear from the newly formed island and soon the entire sea is filled with pumice[1] (see Fig. 5). Similar events continue on the 28th. Finally, on the 29th, the small islet erupts, with the smoke and fire accompanied by lightning and a thunderous sound heard at least 400 km away. Earthquakes continue to shake the island while the ash and pumice reach modern day Turkey. Large ejecta travel more than 8 km in the air and a violent tsunami floods 2 km^2 of land on the eastern coast of Santorini, while also reaching the islands of Ios and Sikinos. Around 70 people lose their lives to poisonous gases and major damage is caused to land, churches, homes and ships by the tsunami [18]. Volcanic activity continues at intervals until early December. The locals name this period of unrest *The Time of Evil*.

[1] Porous, highly vesicular volcanic rock that can float on water (in some cases for one or more years) [21]. Usually white or yellow.

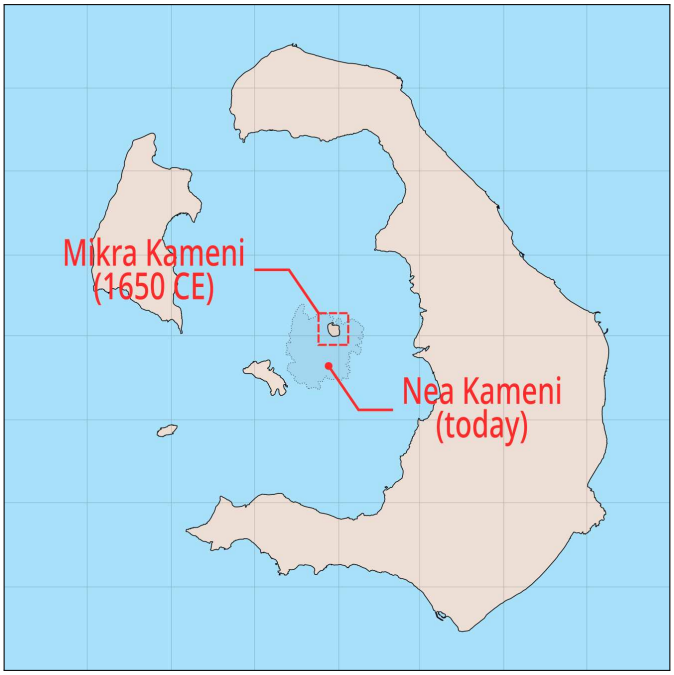

Fig. 4. The island of Santorini around 1650 CE

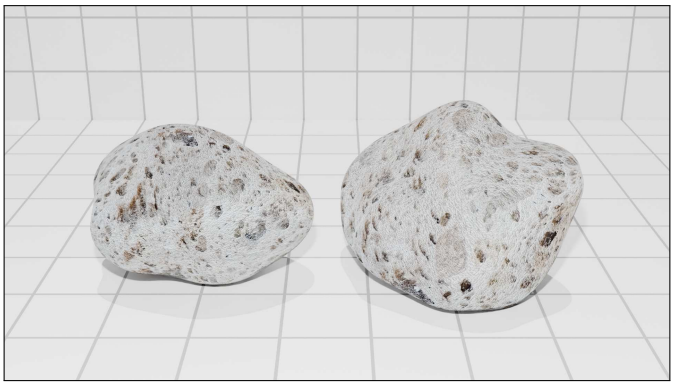

Fig. 5. White pumice stones found across modern-day Santorini (CG render)

Recent Findings

Recent research [19] gives us a better understanding of these events. The islet spotted by the locals was in fact the peak of a submarine volcanic cone. This cone was created after pumice was deposited on top of a pre-existing remnant cone, similar but less abrupt than the one we see today (see Fig. 3). Asymmetries of this pre-existing cone caused the northwest side of the structure to be steeper than the southeast. This lead to a total collapse of the entire northwest flank which generated the violent tsunami.

Importance

Although a major eruption like this one is always preceded by multiple warning signs (e.g. long periods of seismic activity), collapses of submarine structures like the one still present today in the Kolumbo area (see Fig. 3) can happen unexpectedly, e.g. following a major earthquake unrelated to the volcano. An event like that could trigger a major tsunami that would reach the main island in about 5 minutes or a limnic eruption that would spread toxic gases all over the area [19]. This is one of the reasons that increasing the awareness of decision makers and the public about the Kolumbo volcano is crucial.

1.3 Modern Simulation and Visualization Techniques

1.3.1 General Workflow

Introduction

Simulating and visualizing the complex events of the 1650 CE eruption requires a combination of multiple CG tools and techniques. The general workflow for any CG animated production includes *modeling*, *texture painting*, *animating*, *lighting* and *rendering* (see Fig. 6) [22].

Models
Textures
Animation

Accurate to scale 3D models are usually created by hand or using automated techniques like 3D scanning or photogrammetry [23]. For large-scale geological formations, 3D models can also be generated from satellite imagery, while real bathymetry data can be used for the seabed. Realistic textures can be manually drawn, generated from digital photography or composited based on pseudo-random noise patterns. Animations are traditionally manually keyframed, except in the case of natural phenomena where physics simulation techniques allow for procedural generation.

Lighting
Rendering

Proper lightning and shading is achieved using ray tracing techniques. Ray tracing is the approximation of real-world lightning by simulating individual paths of light rays [24]. Depending on the geometry and especially the simulated material of each object on the scene, rays can be reflected, absorbed, refracted or combined with other rays. Modern 3D CG software like Blender [25] ship with built-in ray-tracing based render engines that can take full advantage of the system's CPU(s) and/or GPU(s).

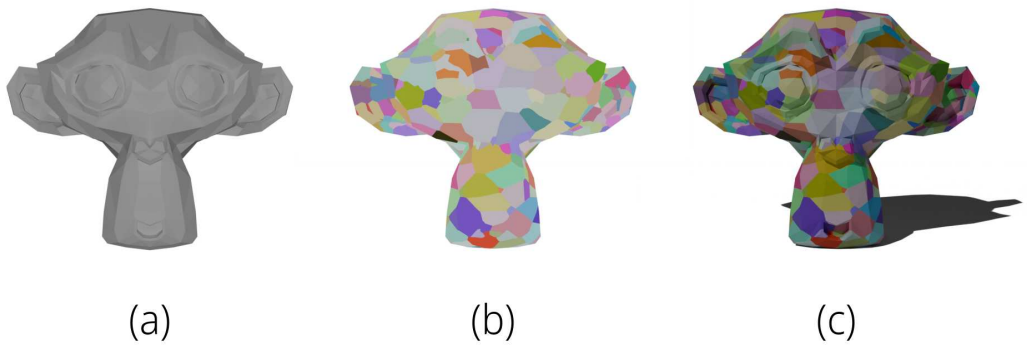

Fig. 6. Results from the process of (a) Modeling (b) Texture Painting and (c) Lighting and Rendering

1.3.2 Computational Physics

Introduction

Visualizing natural phenomena, in most cases, requires simulating the underlying dynamics by solving the Partial Differential Equations (PDEs) that govern them for a sequence of time steps (frames). The methods used for this purpose were initially developed by the *computational physics* community to aid physicist in solving complex problems, acting as a stepping stone between theoretical and experimental physics. With demand for special effects in feature films and realistic movement of objects in computer games rising in recent decades though, new applications for these methods were explored by CG researchers [26].

Physics Engines

Specialized software was developed in order to provide general implementations of different physical systems. These *physics engines* as they came to be known, became a core component of every major game engine [27]. In recent years, physics engines that are able to take advantage of accelerators, like GPUs and TPUs, mainly for use in reinforcement learning, have also been developed (e.g. see Brax [28])

Particles

The simplest form of system implemented in such engines is normally one containing only point masses, usually referred to as *particles* in the field of CG. Each particle has a position, which is updated every frame by a subroutine called the *integrator* based on the first two laws of Newton, and no orientation. Using thousands of such particles, phenomena like flying sparks or falling dust can be simulated.

Rigid Bodies

For larger objects, most applications require only the implementation of classical mechanics, simulating movement and rotation but assuming that the objects are rigid and cannot be deformed. Two distinct systems are engaged in order to properly simulate rigid body physics. One calculates the position and rotation of each object for every frame based on the applied forces, while the other detects collisions between multiple objects in the simulation and updates the forces accordingly.

The effect of the different forces and torques applied can be calculated using only the origin of the object (usually the center of gravity), as no deformation is allowed. Collision detection on the other hand needs to take into account the true shape of the object and can be an extremely complex process. Every pair of objects, sometimes consisting of millions of polygons, needs to be checked for every frame. Modern collision detection techniques take advantage of bounding volumes (e.g. spheres or Oriented Bounding Boxs (OBBs)) or tree-structures to coarsely figure out which objects might be colliding, before moving to a more precise collision detection step by either checking all polygons or recursively applying bounding volumes to both objects [29].

Fluids

Although many objects can be represented as point masses or rigid bodies in computer games and VR applications, most real-world phenomena are inherently more complex. For example, fluids, including liquids and gases, are very common in the natural world and are described by different physical principles than point masses or rigid bodies. Borrowing from the field of Computational Fluid Dynamics (CFD), many ways of discretizing the Navier–Stokes equations which govern most fluid flows of interest in CG have been developed [30].

While Direct Numerical Simulation (DNS) methods that precisely solve the governing equations with enough degrees of freedom achieve the highest level of accuracy, they also require substantial computational resources, making them impractical for many applications. In recent years, multiple Machine Learning (ML) methods that accelerate DNS by correcting coarse simulations or dynamically changing the simulation grid size have also been proposed [31]. Fluid simulations can also be combined with particle physics, where either fluid (e.g. smoke) is emitted from particles, or particles are included in the fluid solver to represent secondary fields (e.g. foam or bubbles).

Soft Bodies Finally, some natural phenomena may require the simulation of deformable objects. Such objects, also known as soft bodies, can move and rotate but also change shape under the influence of external forces. Thus, precise material composition must also be known in addition to the shape and mass which is required for rigid bodies. Operations like collision detection also become surprisingly complex, as bounding volumes cannot be precomputed, and in some scenarios, self-collisions can occur.

One way of modeling such objects, is using a numerical method like the Finite Element Method (FEM), where the PDE governing dynamic elastic materials is directly approximated [32]. However, even if the results are the most accurate using such methods, the increased implementation complexity and computational cost may not always be justified. An alternative method, especially useful when physical accuracy is not a top priority, is based on the Mass-Spring Model (MSM). In this model, the internal structure of the object is approximated using a regularly spaced array of point masses connected by springs or other constraints.

The parameters in MSM are difficult to control and cannot be directly correlated with the material properties of real objects. The volume of the object is also not necessarily preserved, an important consideration for many applications. This has lead to new variants of the MSM with volume preservation constraints [33] as well as the increased popularity of mesh free methods using Lagrangian techniques like Smoothed Particle Hydrodynamics (SPH) [34].

1.3.3 Applications in Geoscience

Mapping and Exploration In the framework of Geoscience, CG and computational physics techniques have found widespread use, especially in the context of 3D mapping and VR applications. Virtual globes, alongside the advancements in GPS and Geographic Information Systems (GISs), sparked a revolution in geological data analysis in the early 21st century [35]. Similarly, recent VR applications allow for better analysis of outcrops by researchers [36] and exploration of underwater environments by the general public [37].

Natural Disasters Substantial work has also been put into modeling tsunamis and their coastal impact [38] as well as photorealistically visualizing them in order to improve understanding [39]. Similar efforts have also been made for urban floods [40], [41], earthquakes [42], [43] and slope failures or landslides [44], [45].

Volcanic Plumes In the field of volcanology, considerable progress has been made in modeling and simulating ash plumes either with numerical models [46] or, more recently, with particle based methods like SPH [47]. Similar methods have also been used to simulate sulfur dioxide (SO_2) emissions from specific eruptions like the one in 2019 on the island of Raikoke [48]. Combined with modern 3D visualization techniques (e.g. see [49]) such simulations could greatly aid the understanding of these phenomena and help mitigate the risks to aviation safety posed by volcanic activity.

Lava Flows Several methods have also been developed for modeling and simulating lava flows [50]. Simulation results have been compared with real lava flow data from the Grand Canary Island (Spain) [51], Mt. Fagradalsfjall on the Reykjanes Peninsula (Iceland) [52] and Kīlauea (Hawaii) [53] with satisfactory alignment in all cases. Us-

ing state-of-the-art frameworks, such numerical simulations of geophysical flows can also be directly visualized and integrated into VR applications [54].

Other Volcanic Phenomena

Other phenomena caused by or occurring during volcanic eruptions have also been simulated. Atmospheric waves (Lamb waves) that circled the earth three times during the 2022 CE Hunga Tonga–Hunga Ha'apai (HTHH) volcanic eruption were successfully modeled using an ocean shallow water model in [55]. Phreatomagmatic activity (interaction of magma with water) has been better understood using a model based on a Finite Volume Method (FVM) in [56]. Finally, multiple volcanic phenomena, including ballistic projectiles, have been recreated as part of a Mixed Reality (MR) application showcasing possible hazards of the Vulcano island (Italy) in [57].

2 Island and Seabed Reconstruction

Related Work Before simulating and visualizing the events of the 1650 CE eruption, an accurate model of the island (see Fig. 4) and the seabed must be reconstructed. In similar past attempts, 3D models of the topography have been created using fairly manual methods. For example, in [57], the Vulcano island model was created using elevation data in a raw image format ported into Unity3D and modified using the built-in Terrain tools. In [58], the Arctic fjord Clyde Inlet (Canada) was reconstructed from multiple data sources and optimized using the Level of Detail (LOD) features of Unreal Engine 4. Finally, the modern day island of Santorini has also been reconstructed in 3D as an example for the creation of an interactive VR experience in [59].

2.1 Digital Elevation Models and Heightmaps

DEMs A Digital Elevation Model (DEM) is a representation of a terrain's surface commonly used in GISs [60]. In their simplest form DEMs are raster images with elevation represented using a single 8-bit color (e.g. see Fig. 7). In the CG world these raster representations are also known as *heightmaps*.

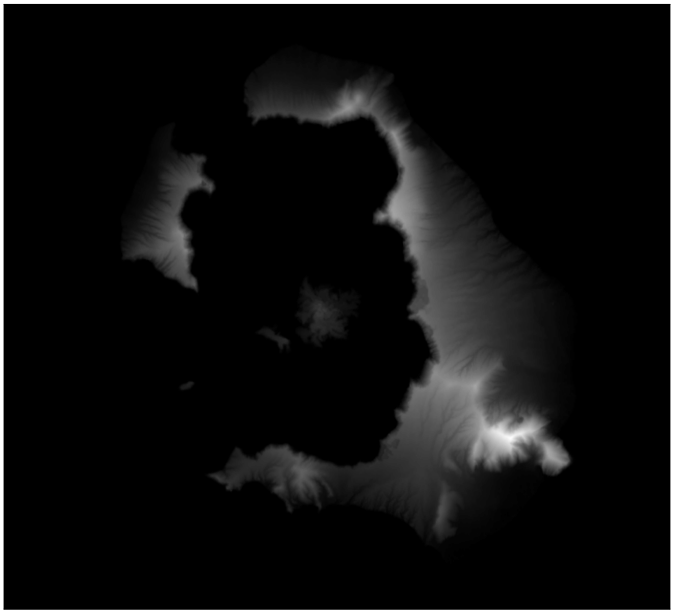

Fig. 7. Heightmap of Santorini with horizontal resolution of approximately 30 meters. Credit: AW3D30 (JAXA)

2.2 Conversion to Usable 3D Models

2.2.1 Basic Methodology and Complications

Data Format

In theory, these images can be very easily converted to usable render-ready 3D models. Each pixel has 2 coordinates (u, v) and a color value c in the range $[0, 255]$. The (u, v) coordinates can be easily scaled to match the real world using a value that accompanies the map, usually indicating *pixels per kilometer* or *meters per pixel*. Similarly, by linearly remapping the $[0, 255]$ color range to the true *minimum* and *maximum height* values, a to-scale 3D point cloud can be created. Finally, considering the nature of the heightmap, which cannot represent cavities, a naive standard grid triangulation is adequate for the conversion of this point cloud to a fully-fledged 3D model.

Complications

Complications arise when we start to consider the real world and the imperfections of remote-sensing satellite data. Let's focus for example on the sea around Santorini in Fig. 7. Although most of it is black (color value of 0), small random noise still exists (e.g. values of 1 or 2). At the same time, the coast (with real elevation values very close to 0) is not clearly defined (for comparison see Fig. 4). Thus, if we want to remove the sea surface from this model, doing so manually is our only option. For example, an outline of the island can be drawn by hand using a vector graphics editor like Inkscape [61] (see Fig. 8) and used like a mask to remove the unwanted topology.

(a) (b)

Fig. 8. Hand-drawn masks of (a) modern day Santorini and (b) 1650 CE Santorini

An unexpected consequence of slicing the model using a binary mask like the one described is that the outer edges become jagged and don't properly contact the zero plane (the water). This can be corrected by selecting all outer vertices (vertices with fewer than 8 neighbors) and manually setting their height to zero. With this final step the process of converting the heightmap to a 3D model is completed (see Fig. 9).

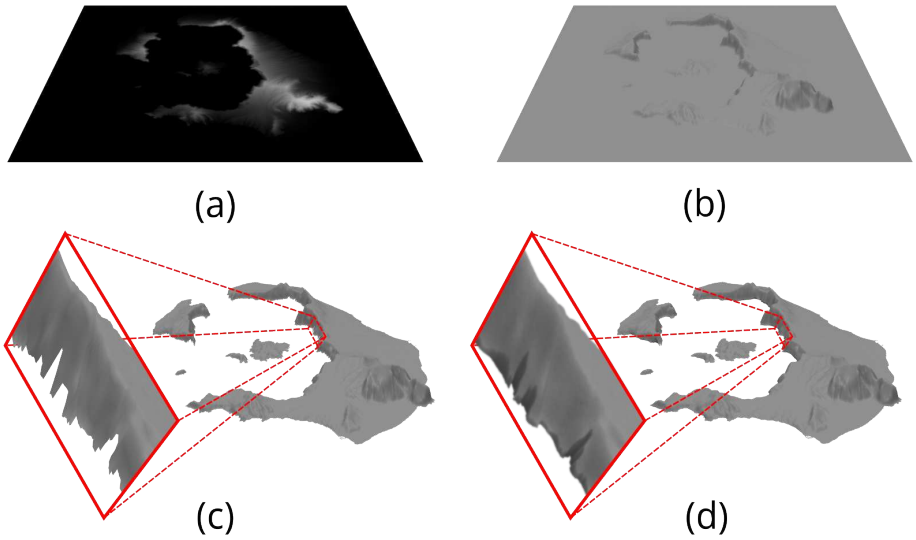

Fig. 9. Heightmap to 3D model conversion
(a) heightmap in 3D space (b) conversion to 3D model (c) application of mask and (d) correction of outer edges

2.2.2 hm2obj: Automatic Conversion

Rationale Although this process can be manually performed using Blender's built-in tools, namely the displace and boolean modifiers and the scaling tool, automating it using a Python [62] script could make the process faster and less error-prone. Based on this reasoning, a raster image heightmap to *.obj* file command-line tool named *hm2obj* was developed[2].

Features The tool takes the heightmap and mask images as input and produces a properly scaled 3D model in the *.obj* format. Additional arguments allow for the downsampling of the input image to reduce the resolution and subsequently the file size of the output, as well as the application of a Gaussian blur filter to make the output model smoother. Correct UV texture coordinates are also produced to allow for use of a satellite image as a texture. Typical execution looks like so:

```
$ ./hm2obj.py -b 10 -d 2 --minz=0 --maxz=567
    --px_per_km=260 -m mask.png -o santorini.obj
    heightmap.png
```

2.2.3 Results

3D models of both 1650 CE Santorini and the current Kolumbo crater (shown in Fig. 3) can now be generated. With the models being to scale, they can also be combined onto a single three-dimensional map (see Fig. 10). This topology is representative of the post 1650 CE eruption topology of Santorini and its northeastern seabed.

[2]Available: `https://www.github.com/GavalasDev/hm2obj`

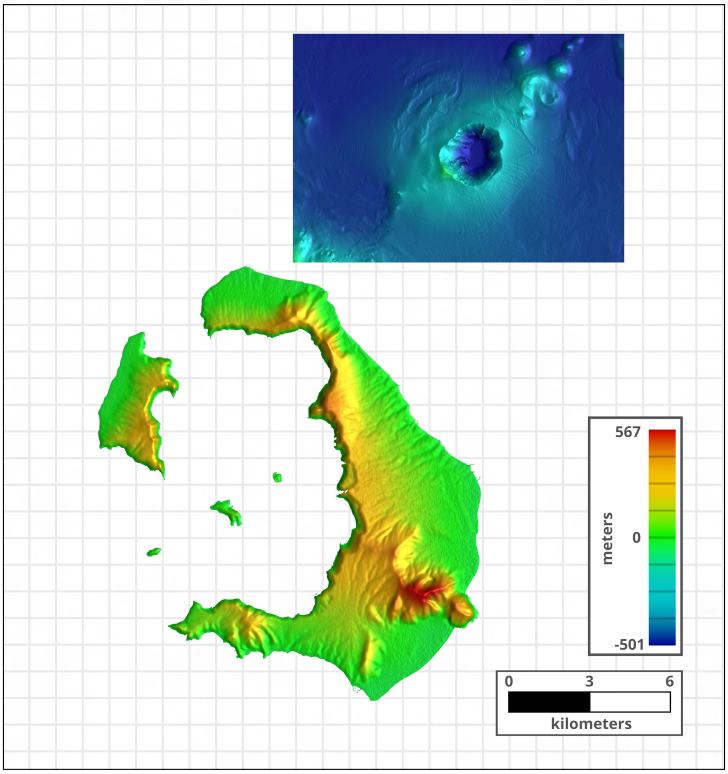

Fig. 10. A post eruption 1650 CE elevation map of Santorini

2.3 Realistic Rendering

Satellite Texture Limitations

In order for the reconstructed models to be usable in the final visualization, realistic textures and materials must also be applied. Although satellite imagery of modern day Santorini could allow for a simple solution to this problem (like in [59]), the island's surface has undergone major changes since 1650 CE, mostly because of increased human activity. For example, the airport north of Kamari, the hundreds of houses in Fira and Oia, as well as the tightly packed well-defined plots of land would all have to be removed by hand. Instead, procedurally generated textures could be employed for the island's surface, decreasing the need for manual intervention while maintaining the realism of the scene.

2.3.1 Procedural Textures in Blender

Introduction

Blender provides several procedural textures for use within its materials system [63]. The node based system (see Fig. 12) allows for the combination of multiple such textures for the creation of realistic materials.

Island Surface

For the island's surface, a Worley noise texture (also known as a Voronoi texture) yields the best results. First introduced by Steven Worley in 1996 [64], the Voronoi texture is great for producing organic textures because of its cell based approach. In the case of Santorini, two different scale Voronoi textures with a green tone are laid over a simple height based brown gradient. Some random smaller scale noise is also introduced to add texture to the otherwise flat 3D models surface. The resulting texture is presented in Fig. 11a.

Sea Surface For the sea surface, standard Perlin noise can be applied as displacement to model the waves. The vector math nodes can be used to animate these waves adding a scalar value to one or more of the coordinates based on the frame number. The resulting texture can be seen in Fig. 11b.

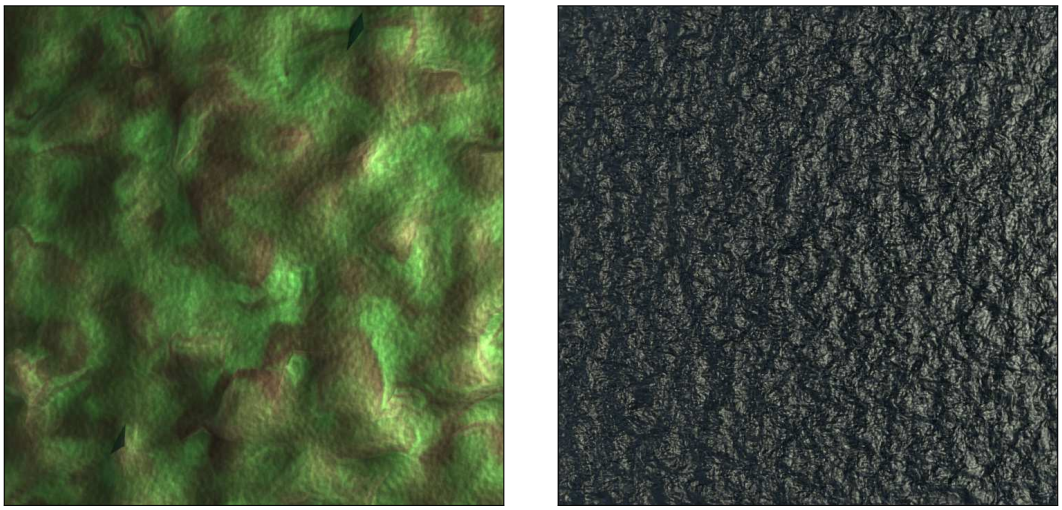

(a) (b)

Fig. 11. Procedural textures for (a) Santorini and (b) the sea surface

2.3.2 Realistic Materials and Illumination

Materials Instead of directly mapping the texture onto the 3D model, a realistic material can be created using Blender's node editor (see Fig. 12). For the island's surface the Glossy Bidirectional Scattering Distribution Function (BSDF) yielded the best results, while for the sea surface the Glass BSDF with the proper Index of Refraction (IOR) for water applied (*1.333*) , was found to be more appropriate.

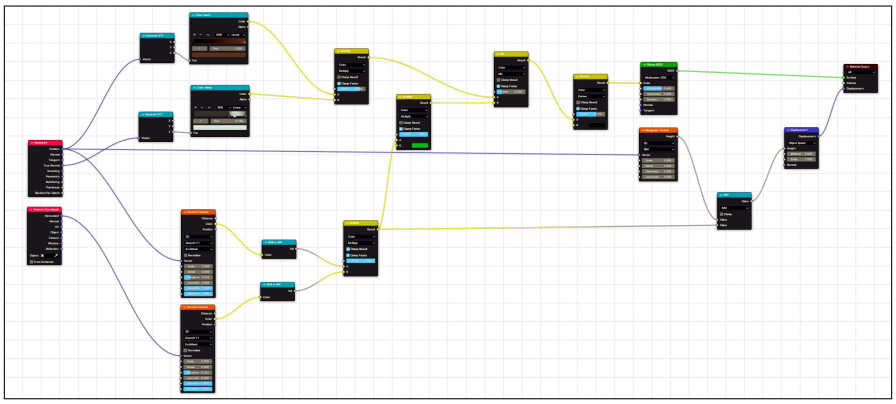

Fig. 12. Realistic surface material in Blender's node editor

Sky Texture For proper illumination of the scene, a procedurally generated sky texture based on Nishita's model [65] provided by Blender was employed. This allows us to control and animate the sun's size and location as well as the air's quality.

2.3.3 Results

With these materials applied we can now render a simple scene with the 3D model of Santorini atop a zero-height plane acting like the sea. The results, for different times of day, can be seen in Fig. 13.

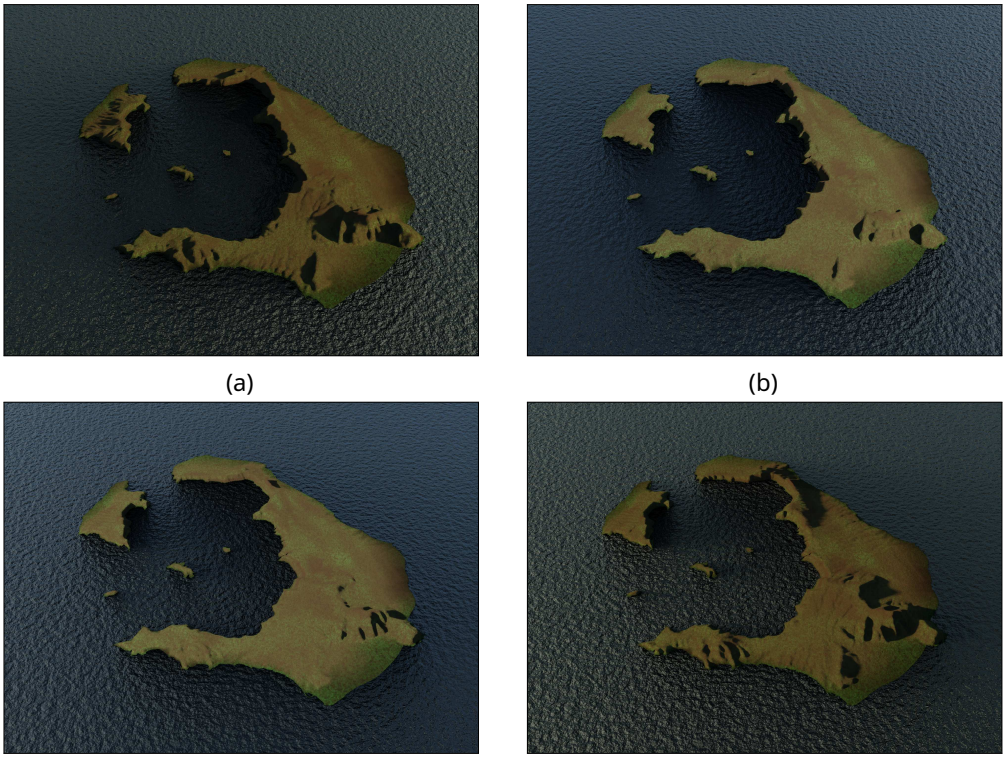

(a) (b) (c) (d)

Fig. 13. Renders of 1650 CE Santorini at different times of day

3 Subaerial Phenomena

Introduction

With a render-ready model of Santorini and the modern-day Kolumbo crater reconstructed, we can now start examining the subaerial phenomena of the 1650 CE eruption. Naturally, most reported phenomena by first-hand witnesses belong in this category. The most important ones include the volcanic plume, accompanied by lightning and sounds of thunder and the major tsunami.

The 2022 HTHH Eruption

To get a better understanding of how these events played out during the 1650 CE Kolumbo eruption, we can turn to the most recent comparable-scale submarine volcanic eruption, the 2022 CE eruption of the HTHH volcano. Being closely monitored with modern technology, this HTHH eruption provides a significant opportunity to better understand past eruptions as well as future risks [66]. By combining videos of the eruption and the subsequent tsunami with data from satellite observations, we can accurately determine the scale of various phenomena and their characteristics.

3.1 Volcanic Plume and Smoke Simulations

Volcanic Plume

The most prominent subaerial phenomenon in any volcanic eruption is the generation of an eruption column or plume. Volcanic plumes are primarily composed of volcanic particles, gases, and entrained air and have different characteristics based on the type of eruption. Their unique structure and shape is mostly controlled by the initial vertical momentum and the effect of buoyancy [67].

In the field of CG, effective simulation and visualization methods for such plumes have not been widely studied, with smoke and clouds being the closest well-researched analogous phenomena. However, the scale and complexity of volcanic plumes introduce unique challenges that are not present in these smaller-scale phenomena. For example, the 2022 CE eruption of the HTHH volcano generated a plume that rose 58 km in height and eventually covered an area of 157 000 km^2. This massive scale, coupled with the unique dynamics of volcanic plumes, makes standard grid-based fluid simulations (such as those used for smoke) inadequate for accurately modeling this phenomenon.

In [68] these challenges where tackled using a layered animated model working at different scales. First, for simulating the large-scale shape and dynamics of the plume, a cone is created from a series of cylinders, growing in radius the further away they are from the volcanic vent. Then, smaller-scale turbulent flows are simulated within these cylinders, filling the gaps and adding randomness to the cone shape. The umbrella shape created over the plume is simulated with the top cylinder effectively growing in radius after reaching a certain height.

In this work, a similar two-layered simulation model was explored using the built-in tools of Blender. In particular, a guided particle system is used instead of a series of cylinders for the creation of the cone shape, as well as the umbrella. The particles are emitted with a large upward velocity from a hemispherical shape with randomness applied to their normal-facing velocity. Gravity simulation for the particles is disabled. Once they reach a specific height a force is applied, effectively rotating them and creating the expected umbrella shape (see Fig. 14a). Each particle slowly emits smoke during its entire trajectory to fill in the gaps. Turbulence

is added to this smoke to give the plume a realistic shape at all scales.

Rendering Rendering methods used for objects with volume, like in this case smoke, vastly differ from the standard rendering methods used for solid objects. Volume objects are represented not by an array of primitives like triangles, but by a set of samples of some property (e.g. density) at different 3D locations. These samples, more commonly known as *voxels*, are arranged in complex data structures that make it easy, and more importantly fast, to parse through them during simulation and rendering [69]. The most common such data structure, named VDB, was originally developed by DreamWorks Animation, and released to the public in 2012 as OpenVDB [70].

In Blender, a more recent iteration of VDB released by NVIDIA called NanoVDB [71] is currently being used for rendering volumetric objects. The major benefit offered by NanoVDB is that it can leverage the system's GPU for improved computation and rendering speeds, unlike OpenVDB which is limited to the CPU. To work with the already present ray tracing engine, a bounding mesh is used to determine whether a ray is inside the volume, at which point the NanoVDB structure is used for sampling [63]. In practice, in order to get a realistic render we just have to apply a volumetric material to our smoke object (see Fig. 14b).

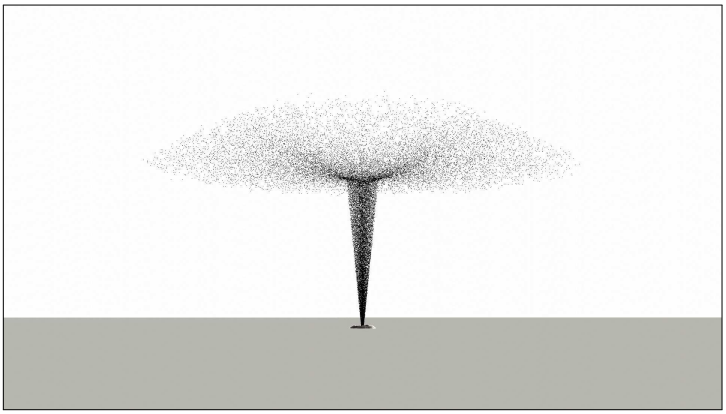

(a)

(b)

Fig. 14. (a) The shape of a volcanic plume in the absence of wind modeled using particles and (b) Volcanic plume rising over the sea surface (CG render)

Animation and Tuning

The use of smoke emitting particles for the simulation also allows for animation of the entire lifetime of the plume (see Fig. 15). Although the final rendering of each frame is computationally more expensive than [68], where one of the goals was real-time interactivity, the particle simulation which effectively controls the shape of the plume can run in real time. This allows for rapid prototyping and iterative refinement of the plume's dynamics. Blender's force fields can also be used to simulate environmental effects such as wind or turbulence at different heights further enhancing the realism of the final visualization.

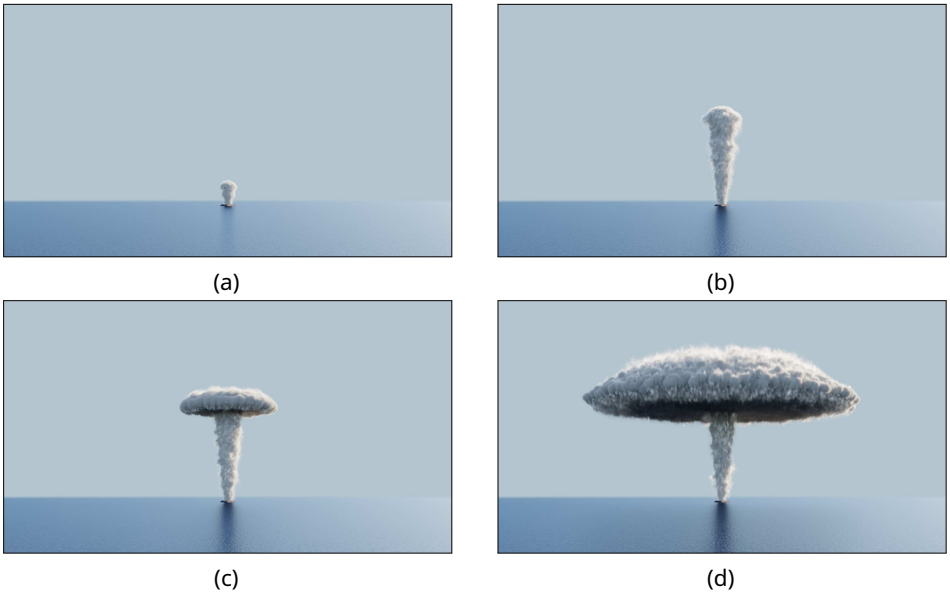

Fig. 15. Four frames from the lifetime of a volcanic plume as simulated using smoke-emitting particles

Other Smoke Simulations

Examining available footage from the events leading up to the eruption of the HTHH volcano in 2022 CE (e.g. see [72]) more phenomena that could be simulated in a similar manner are observed. This includes multiple smaller, dense bursts of dark ash and ejecta. In this case, by having gravity affect the emitted particles realistic individual trajectories can be generated. The trailing smoke can also have a diminishing density value, making the effect appear more natural. The result can be seen in Fig. 16.

Fig. 16. Burst of dark ash ejected from within the sea (CG render)

3.2 Tsunami Simulation and Visualization

Introduction

Volcanically generated tsunamis are inherently complex and fundamentally different from those caused by earthquakes, which are better understood by scientists. One reason for that is that they can arise from various source mechanisms, including underwater explosions, pyroclastic flows, slope instabilities and caldera collapses [73]. Specialized software like VolcFlow [74] has been developed to simulate the dynamics of volcanically generated tsunamis.

Shore Interaction

Tsunami-shore interactions, although very important for correct risk assessment, have been traditionally very hard to simulate. In open waters, tsunamis propagate undisturbed and can be very effectively described using 2D nonlinear equations. Once they reach the shoreline though, the waves instantly become turbulent and multiphase, by interacting with the sand, dirt and other debris, making them much more complex [38]. Realistic visualizations are also hampered by the need for high-fidelity models of the coast.

In the case of Santorini, although accurate 3D models of the modern-day coast could be created using Unmanned Aerial Vehicles (UAVs) and photogrammetry techniques (like in [75]), significant modifications would have to be made to recreate the 1650 CE coastline. In addition, detailed bathymetry data would need to be acquired close to the shoreline, as the seabed morphology greatly impacts the behavior of incoming waves [76]. Due to these complexities, along with the increased computational and resource requirements, such finer-scale simulations fall beyond the scope of this work.

Visualization

Even without a physically accurate simulation, we can easily create an animation showcasing important details about a tsunami, like the propagation speed, amplitude and wave direction. This can be achieved using animated, procedural wave textures applied as displacement on the sea surface. By properly keyframing the movement of the texture, the timing of the waves can be matched to real observations or theoretical predictions. Similarly, the strength of the displacement can be used to match the expected wave amplitude. A wave texture procedurally generated from Blender along with the resulting effect on the sea surface is showcased in Fig. 17.

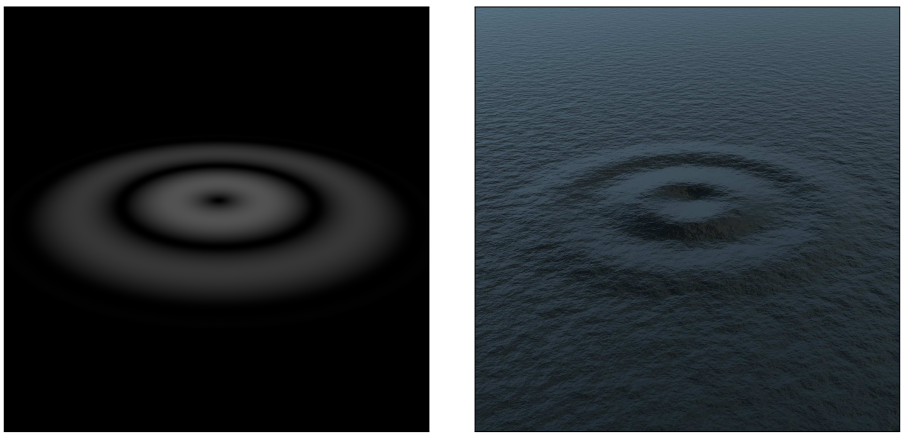

(a) (b)

Fig. 17. Procedural wave texture (a) visualized as a heightmap and (b) applied to the sea surface as displacement

3.3 Secondary Phenomena

Earthquakes

In the lead-up to an eruption, as pressure increases in the magmatic chamber, episodes of volcanic unrest intensify. These events are defined by ground deformation, changes to the hydrothermal system and more importantly, frequent earthquakes [77]. In the case of Kolumbo's eruption in 1650 CE, earthquakes where experienced by the inhabitants of Santorini up to a year prior, with some even considering fleeing the island [18]. Better understanding of the connection between earthquakes and volcanic eruptions could thus be crucial for risk mitigation efforts.

While detailed visualizations of the effects of earthquakes can be achieved using CG techniques (e.g. see [78]), more practical methods were considered for this work. For example, a simple animation of the rotation of the camera using random, periodic oscillations can be a satisfactory method for conveying the duration and intensity of an earthquake, as well as its relation to the volcanic activity.

Lightning

Another phenomenon reported during the 1650 CE eruption of Kolumbo is thunder-like lightning around the eruption column. This is now known to be pretty common for all kinds of eruptive activity and is considered an intrinsic property of volcanic ash plumes [79]. Volcanic lightning is particularly interesting to scientists because it enables the use of pre-existing lightning detection instruments for eruption monitoring [80]. Lightning during volcanic eruptions is also an additional hazard, with some incidents even resulting in fatalities in previous eruptions [81].

In CG, lightning is usually visualized using procedural textures because of its two-dimensional nature. Models are created either empirically using random tree-like patterns or based on physical simulations for increased realism [82]. Scattering effects due to atmospheric particles or clouds have to also be taken into account for proper illumination effects of the scene [83].

Sound

Another major element of volcanic eruptions is the produced rumbling sounds. During the peak of the Kolumbo eruption, the generated sounds were heard at least 400 km away in modern-day Turkey while, on the island of Chios about 200 km away, inhabitants thought that the sounds were canon fire and a naval battle was taking place in the vicinity [18]. During the more recent HTHH eruption the audible sound reached Alaska, 10 000 kilometers away.

Sounds for use alongside CG visuals are usually based on real audio recordings layered and enhanced with digital effects. Methods for animation-synchronized explosive sound synthesis have also been developed [84]. Exploring these methods in the context of volcanic eruptions, where sound generation is significantly more complex and influenced by many factors, could be an interesting addition to the introduced visualization methods, but this lies beyond the scope of this work.

Other Phenomena

Other subaerial phenomena could also be simulated and visualized to add details and improve realism. For example, the sea reportedly changed color, gaining a green tint around the Kolumbo area before the major eruption. This could easily be visualized using a texture laid over the sea surface. Large ejecta could be visualized using particles and procedurally generated meshes. Similarly, pumice traveling on the sea surface could be modeled using particles and simulated wind forces. However, recent research efforts indicate that the most interesting aspects of the Kolumbo eruption are in fact submarine.

4 Submarine Phenomena

Significance Modern understanding of volcanic eruptions reveal that most of the reported subaerial phenomena during the 1650 CE Kolumbo eruption are merely manifestations of more complex processes occurring below the sea surface. The earthquakes felt in the months leading up to the eruption were results of the pressure buildup in the magmatic chamber. The newly formed island spotted by the locals was only the top of a submarine volcanic cone, created from pumice deposits over the course of two weeks. Finally, the tsunami that majorly impacted the surrounding islands was triggered by a collapse of the northwestern flank of this submarine cone [19].

Challenges Visualizing these submarine phenomena is essential for enhancing our understanding of the 1650 CE Kolumbo eruption, despite the inherent challenges involved. One of these challenges is limited visibility underwater, something that is considerably augmented by the massive scale of the Kolumbo field. The present-day crater extends 2500 meters wide and 500 meters deep (see Fig. 3). This scale makes a truly realistic visualization of the underwater events an unattainable goal. Of course, we can overcome this challenge by sacrificing some of the scene's realism, improving visibility of the phenomena wherever necessary.

4.1 Seabed and Hydrothermal Vents

Seabed Before visualizing the events of 1650 CE, we can start by modeling the modern-day Kolumbo volcanic field. A render-ready 3D model of the seabed was created using the techniques described in Section 2. Explorations of the crater floor of Kolumbo using Remotely Operated Vehicles (ROVs) though, reveal a much more interesting topology than the one pictured by the bathymetry data alone.

Vents At the crater floor, 500m below the sea surface, exists an active hydrothermal vent field, first discovered in 2006 CE [85]. This field is characterized by several hydrothermal chimneys, discharging gasses and high-temperature fluids with temperature readings as high as 220 °C. These continuously and vigorously discharged gasses are primarily composed of CO_2 [86]. By inspecting videos from ROV explorations of the area (e.g. see [87]) we can easily recreate the most important aspects of these hydrothermal vents.

The rock formations present in the hydrothermal vent field of Kolumbo are defined by a brownish red color and complex shapes. A material can be created for these rocks based on procedural textures using the methods described in Section 2.3.2. Their shape can be recreated using procedural methods like in [88] or, more practically using the sculpting tools of Blender. By far their most distinctive characteristic though is the constant stream of gas bubbles flowing upward, in some cases fairly violently. This animated stream of bubbles can be easily recreated using particles with an initial upward velocity. Two examples of recreated hydrothermal vents can be seen in Fig. 18.

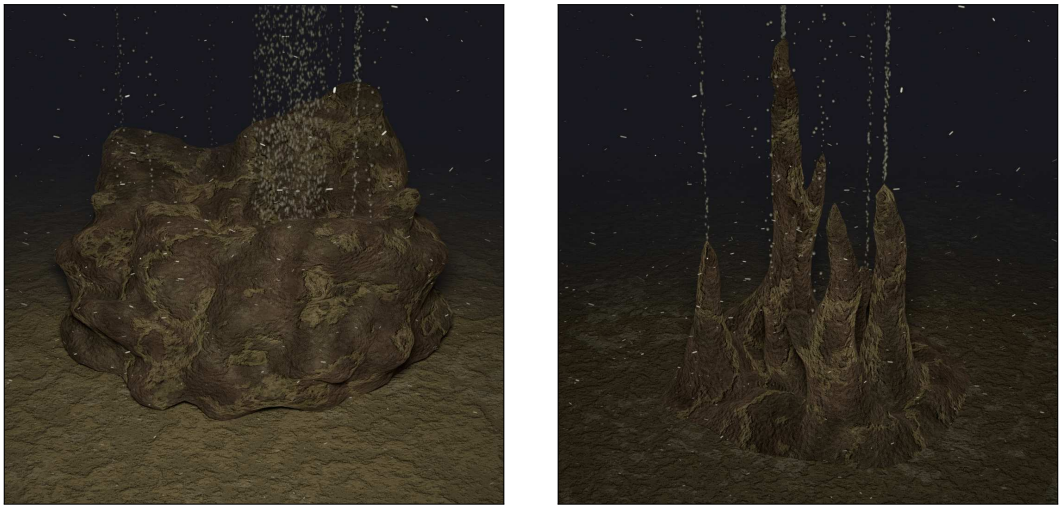

Fig. 18. Two example rock formations from the Kolumbo hydrothermal volcanic field (CG render)

4.2 Cone Formation

Introduction

Along with the earthquakes leading up to the major eruption of 1650 CE we now know that a volcanic structure was forming beneath the sea surface atop a pre-existing crater. This structure was probably cone-shaped and was built over the course of two weeks by pumice deposits. Because of the asymmetries of the pre-existing crater the northwestern flank of this cone was steeper than the south-eastern flank [19].

Simulation Difficulties

Accurately simulating and visualizing this phenomenon requires significant computational power because, although a formation time of two weeks is extremely short in geological terms, it is quite long for numerical simulations. Additionally, an accurate model of that pre-existing crater would be necessary. Although 3D seismic techniques allow for the analysis of the surface below the 1650 CE deposits, only a remnant of the pre-existing cone can be retrieved in this fashion. Thus, a more practical approach is considered.

Practical Visualization

Effective visualization of the cone formation process can be achieved without real simulation data. The pre-existing crater can be manually modeled as a shallower version of today's topology. Then, particles can be used once again to model the pumice being deposited atop this pre-existing crater. As these particles collide with the crater mesh we can animate the crater's scale and shape using keyframing methods (i.e. make the model grow in the vertical direction as time progresses). This way a satisfactory result can be achieved without the need for realistic numerical simulation. A few frames from the cone formation process as visualized using this technique can be seen in Fig. 19.

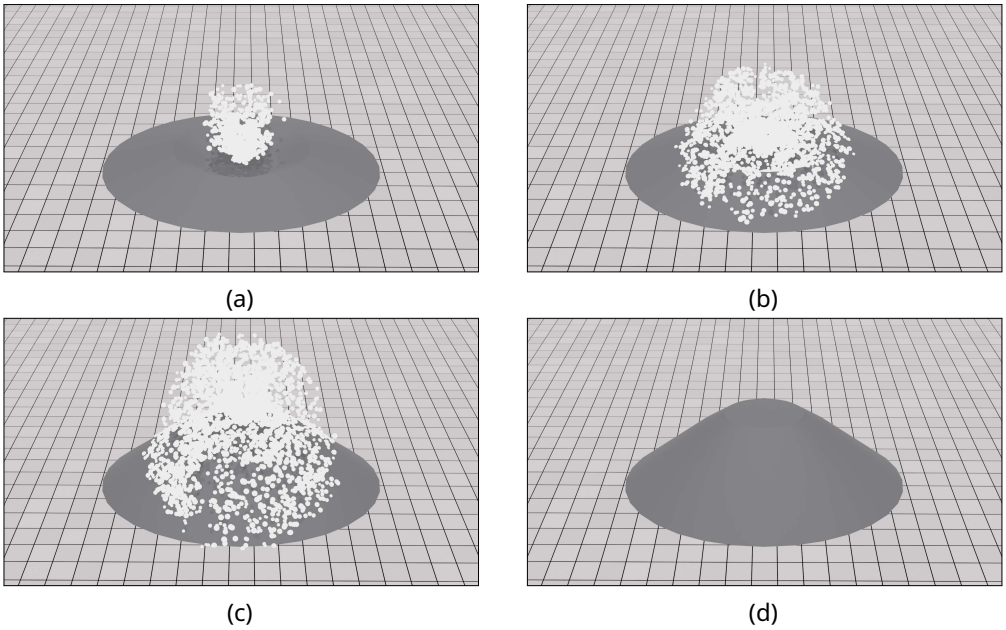

Fig. 19. Four frames from a simulation of the formation process of a volcanic cone

4.3 Flank Collapse

Introduction

Possibly the most important phenomenon that occurred during the 1650 CE eruption of Kolumbo is the collapse of the northwestern flank that triggered the major tsunami with reported maximum run-up heights of up to 20m. Like previously detailed, this flank instability occurred because of the asymmetries present in the pre-existing crater on top of which the cone was formed from deposited pumice. This theory, recently proposed in [19], is supported by numerical tsunami simulations as well as by the modern-day topography of the Kolumbo volcanic field.

NW Flank

Focusing on the northwestern topography of Kolumbo, two distinct features that suggest a past collapse can be identified. The first one is a series of curved ridges, indicative of down-slope compression, that run through the northeastern side in comparison to the relatively smooth southeastern flank. The second one is a well-defined, smoother surface towards the top of the volcanic crater which matches the expected profile of a detachment surface due to flank instability (see Fig. 20). Combined, these features paint a fairly clear picture on how the northwestern flank collapsed.

Tsunami Generation

This collapse is thought to have happened during the height of the eruption. The large movement of material had two direct consequences. First, a directed tsunami was created towards the northwest, away from Santorini, following the movement of the slope. At the same time, the collapse exposed the magmatic system to seawater, leading to depressurization and phreatomagmatic interactions. This change to the dynamics of the eruption, caused a second, this time radial, tsunami. Numerical simulations show that the combination of these two tsunamis agree with first-hand reports across the impacted islands.

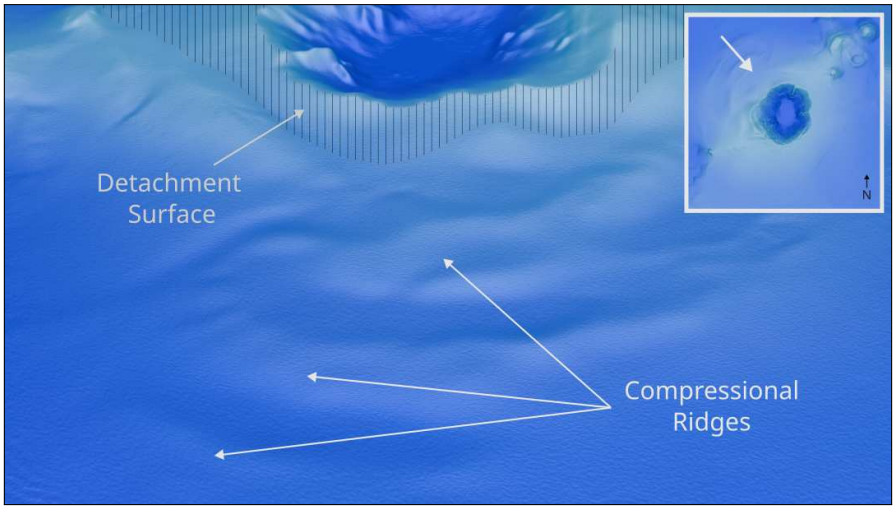

Fig. 20. Northwest side of today's Kolumbo crater (visualization of bathymetry data)

Simulation Difficulties

Similarly to the cone formation phenomenon, even though the time frame is much shorter, this flank collapse is difficult to accurately simulate and visualize. Numerical methods like the smoothed particle FEM which have been used in related work (e.g. see [44]) produce detailed results but are hard to integrate into a realistic rendering pipeline. At the same time, a keyframe-based solution like the one presented in the previous section cannot be employed because of the inherent complexity of the movement involved. An effective intermediary solution is to manually define the detachment surface and treat the flank as a soft (deformable) body.

Simulation of deformation and soft bodies is traditionally a difficult problem in CG because objects are not usually represented with an internal structure. Instead, a mesh representing the surface of each object is created using primitives (usually triangles) and a hollow interior is assumed. This is why a separate model, like the ones described for soft bodies in Section 1.3.2, needs to be employed. Before proceeding with this simulation though, a model of the cone with the detachment surface and flank properly defined needs to be created.

4.3.1 Volcanic Cone Model

Modeling

As the real shape of the volcanic structure is unknown, a primitive cone shape can be used. In order to use soft body simulation techniques to simulate the collapse, this cone shape has to be separated into two distinct parts. The first one will remain static during the entire simulation while the second will act as our deformable object. The exposed part of the detachment surface present today in the Kolumbo crater has a slope angle of about 19°. This, combined with the assumption that the subaerial vent (island) slid into the sea along with the flank allows us to estimate a probable separation plane (see Fig. 21).

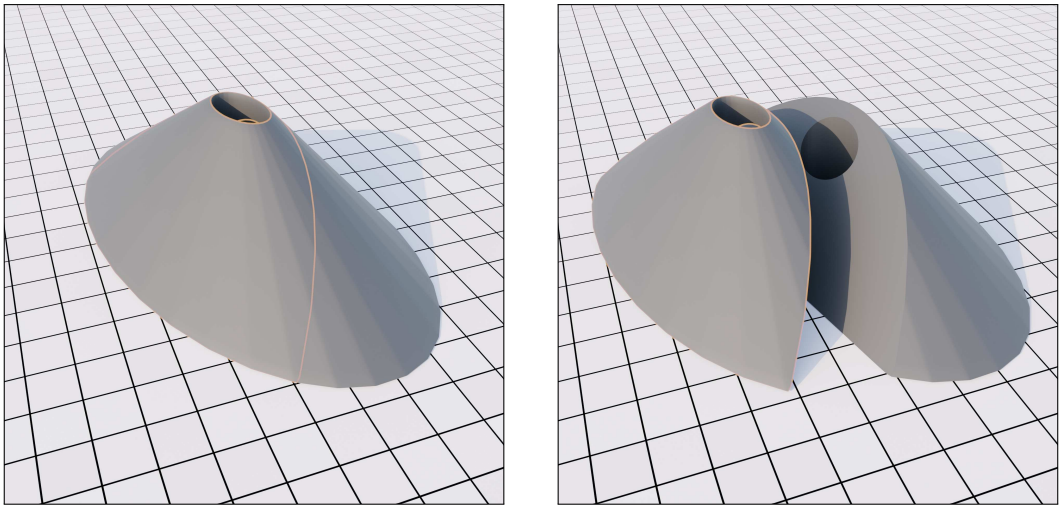

(a) (b)

Fig. 21. (a) Complete and (b) separated 3D model of the volcanic cone (dynamic part outlined in orange)

Collisions Collision planes are also added for the floor and the detachment surface as shown in Fig. 22. Like detailed in Section 1.3.2, collision detection is a computationally intensive simulation step, especially for deformable objects. Using primitive shapes like planes substantially decreases the complexity of collision detection without majorly sacrificing accuracy. Essentially the static part of the cone model becomes invisible to the physics engine, with the collision plane (shown in red in Fig. 22) taking its place.

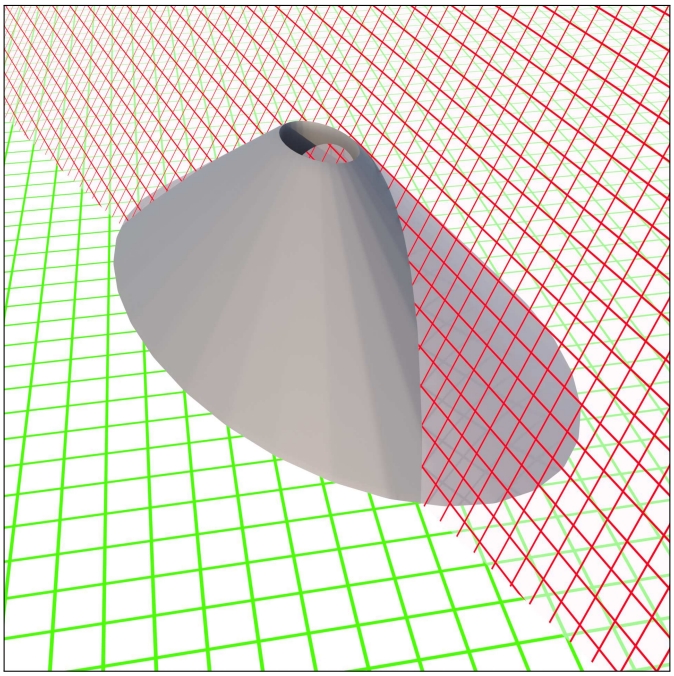

Fig. 22. Visualization of the collision planes defined for the flank collapse simulation

4.3.2 Simulating Using Existing Tools

External Physics Engines

Most physics engines, included in game engines like Unreal Engine [89], animation software like Houdini [90] or distributed as standalone software like Bullet [91] natively support soft body simulations. Use of one of these engines though would require a process for moving data to and from Blender as that is where our rendering pipeline has been set up.

Object data could be exported from Blender using the Graphical User Interface (GUI) or the provided Python Application Programming Interface (API). The data could then be passed to the physics engine for the simulation to take place. After all the simulation steps are complete, most physics engines allow for the storage of the simulation data in a binary or text-like format. This process is usually referred to as *baking*. This baked simulation data could then be accessed using the Python API in blender and the objects updated before rendering every frame.

Blender's Physics Engine

Of course, this process could lead to a lot of pitfalls, as data storage formats are not universal among 3D CG software. To avoid this, the internal blender physics engine could be used instead. Blender's physics engine natively supports soft-body dynamics along with particles, fluids, rigid bodies and others. Blender uses the Mass-Spring Model (MSM) for the simulation of soft bodes, described in Section 1.3.2, with stiffer surface springs to maintain the object's initial shape [63].

The issue with using Blender's built-in physics engine for our case is that the soft-body tools have been optimized for simulating elastic objects like rubber or gelatin. At the same time, most parameters of the internal model cannot be directly altered. Deformation can be enabled and controlled only using a single parameter, called *plasticity*, which affects the behavior of the springs. Even in that case though, a gelatin-like bounciness is inherent to the internal spring structure and is always observed (see Fig. 23). Thus, realistic results cannot be achieved using this technique for our use case. To match the dynamics of the collapsing flank, a more robust system needs to be developed.

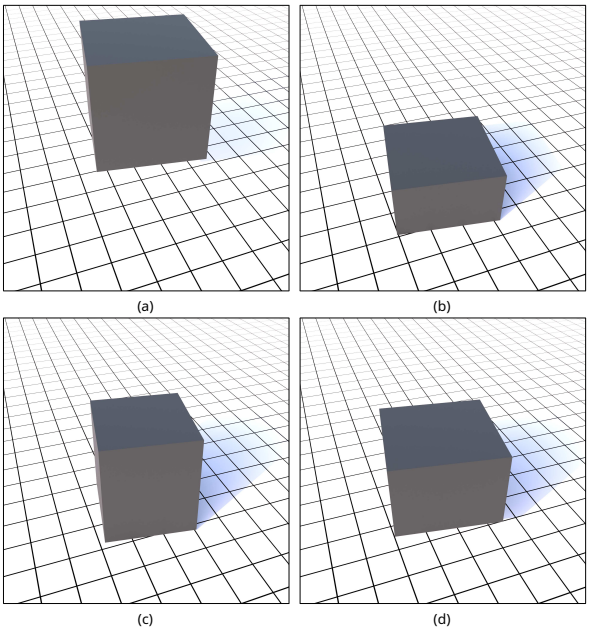

Fig. 23. Four frames from a soft body simulation using Blender's built-in engine

4.3.3 Use of Rigid Body Physics for Mesh Deformation

Summary Although the soft-body physics engine of Blender does not meet our needs, the powerful Python API allows us to develop a custom solution. Instead of relying on an external physics engine and porting the simulation results to Blender, the rigid bodies subsystem of Blender's physics engine can be directly used to model the collapsing flank using a model similar to the MSM. Then, using the Python API, the rigid body simulation results can be used to modify the flank mesh, giving the impression of a deformable object.

Internal Model As described in Section 1.3.2 the standard MSM approximates the internal structure of an object using an array of interconnected point masses. Collision detection in that case becomes inherently more complex, not only because self-collisions are now introduced as a potential issue, but also because a bounding shape for the object cannot be precomputed. In our case, where accurate collision detection is not a top priority, an alternative model can be used. Instead of point masses, rigid spheres can act as the building blocks of the mesh. Thus, by only calculating collisions based on these spheres and ignoring the surrounding mesh, collision detection becomes greatly simplified.

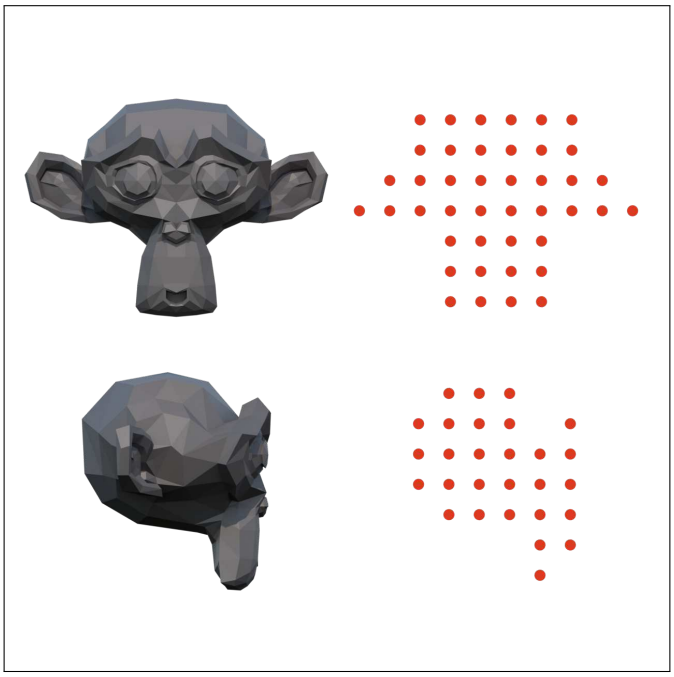

Fig. 24. Internal structure of 3D object represented by regularly spaced rigid spheres

The number of spheres used to model the internal structure of the object depends on the expected result. An example object with the grid of spheres (shown in red) representing its internal structure is shown in Fig. 24. The position and rotation of these spheres can now be calculated over time based on classical mechanics for each frame of the simulation using the rigid body engine. Of course, with the only force acting on these spheres being gravity (and friction during collisions) and nothing to maintain their structure, the resulting movement cannot be used to model a deformable object (see Fig. 25).

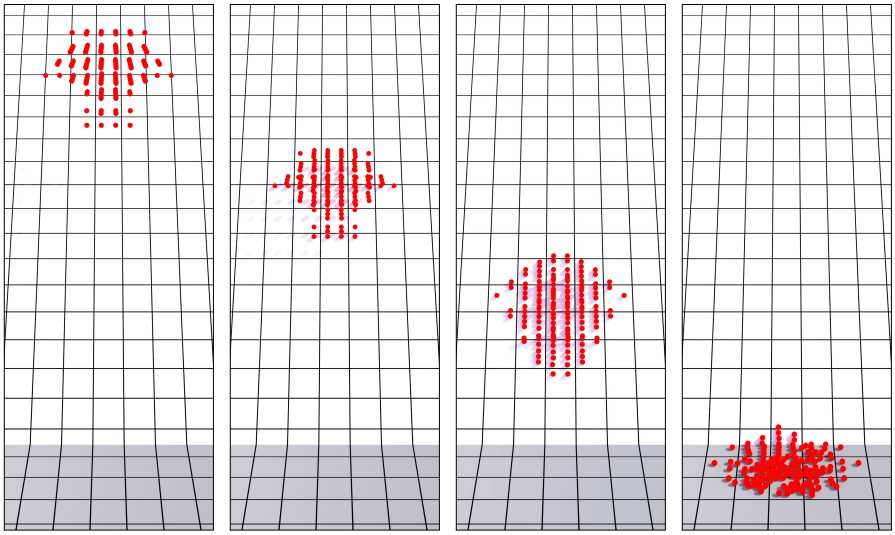

Fig. 25. Rigid body simulation of unconnected spheres

Number of Connections

To create a proper internal structure the spheres have to be interconnected. For the best overall results, it was found that every sphere should connect to every one of its neighbors, including diagonal ones. This means that, for a cube-like three-dimensional grid with n spheres on each side, like the one shown in Fig. 26, the total number of connections is:

$$connections = \frac{1}{2}(26(n-2)^3 + 102(n-2)^2 + 132(n-2) + 56)$$

This formula can be derived by summing the number of connections of each sphere based on the four distinct possible positions outlined in Fig. 26.

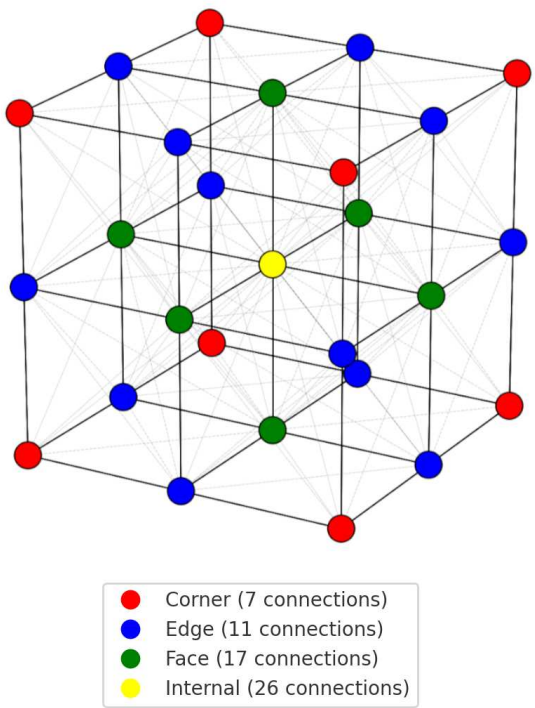

Fig. 26. Connections between neighboring spheres arranged in a 3x3x3 grid

The cubic relationship between the grid size and the number of potential connections limits us to smaller grid sizes for the representation of objects, as more connections increase computational complexity and thus simulation times.

Types of Connections

As the name implies, the standard MSM uses springs for the connection of the distinct point masses. This is great for modeling objects with a tendency to recover their shape after collisions but not really ideal for deformable objects. In our case for example, no elasticity is necessary as all deformation to the flank as it collapses is permanent. Instead of springs, it is thus considered more appropriate to use simple *constraints* between neighboring spheres. These constraints can be linear, or angular.

Linear constraints limit the distance between the connected spheres to a certain range in each axis. Similarly, the angular constraints limit the angle formed between the connected spheres. Every pair of spheres is connected by both types of constraints for maximum control. Larger limits for these constraints allow for a larger range of movement between the spheres, and thus more effective deformation. Repeating the simulation of Fig. 25 with constraints placed in the movement of the spheres as described yields the results shown in Fig. 27. The initial shape of the object is retained while deformation is also properly applied.

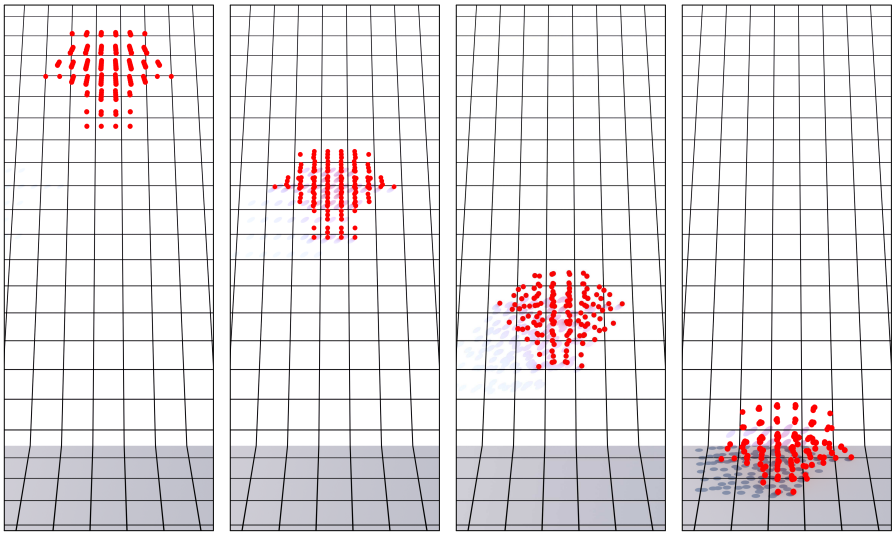

(a) (b) (c) (d)

Fig. 27. Rigid body simulation of spheres with movement constraints

Skinning

In order to go from the sphere simulation to the final mesh animation, a technique called *skinning* can now be applied. Skinning, traditionally used in skeleton-based animations, is the process of wrapping a mesh around a set of control points, in this case the spheres. Like previously detailed, every object in 3D CG is compromised of a hollow mesh, made out of primitives (usually triangles). Thus, in order to move an object, we have to move the vertices that make up these primitives.

In the simplest form of skinning, before the simulation starts and while the object is at rest, every vertex of the mesh is associated with its closest sphere. During this association phase the position of the vertex relative to the sphere is stored as a three-dimensional vector. Then, before the rendering step of each frame the position of each vertex is updated by adding this vector to the position of the as-

sociated sphere. This way, the distance of each vertex with its associated sphere is kept constant, and the mesh follows the spheres.

During the rigid body simulation though, even if it's not visible in the renders, the spheres also rotate based on the torques applied to them (e.g. friction). This rotation must also be taken into account during the skinning process. Before the vector, stored during the association phase, is added to the sphere's position, a rotation equal to the current rotation of the sphere relative to its initial position must be applied. The differences between making and not making this correction are demonstrated in Fig. 28.

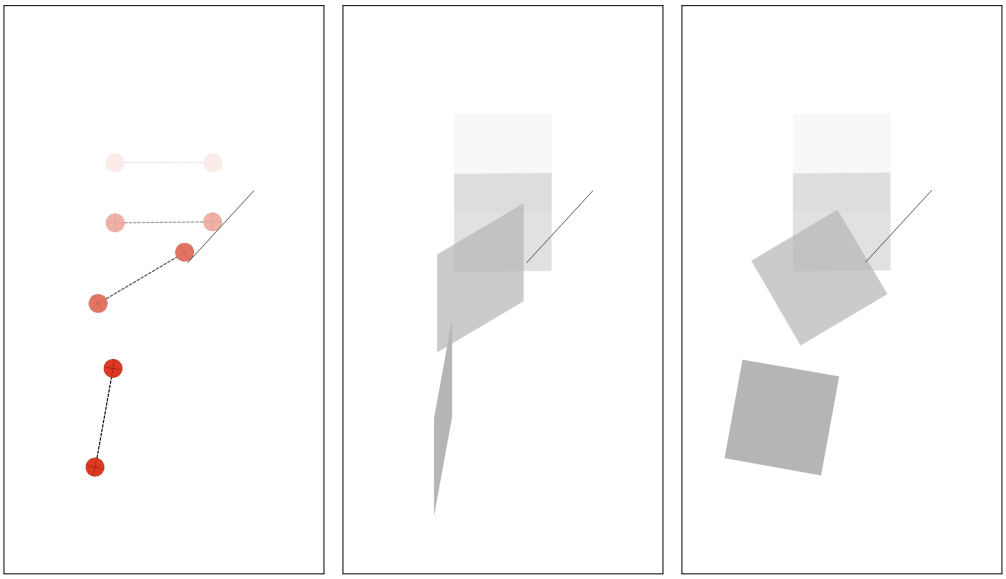

(a) (b) (c)

Fig. 28. Soft body simulation of a cube based on two rigid body spheres (for illustration purposes). (a) control spheres and constraint (b) cube without rotational correction and (c) cube with rotational correction

A final improvement that can be made to the skinning process, is taking multiple spheres into account during the association phase. Specifically, instead of focusing only on the closest sphere, we can store the position of each vertex relative to the n closest spheres. Then, before rendering the frame, a new position for the vertex can be calculated like before based on each of the n spheres. By averaging the coordinates of these calculated positions, a final new position can then be determined. This allows for smoother skinning of the mesh, without harsh edges.

Using this skinning method on the sphere simulation of Fig. 27 and the mesh shown in Fig. 24 we now observe the expected deformation applied to our object (see Fig. 29). This skinning step completes our custom deformable object simulation pipeline, and we can now move back to simulating the flank collapse of Kolumbo.

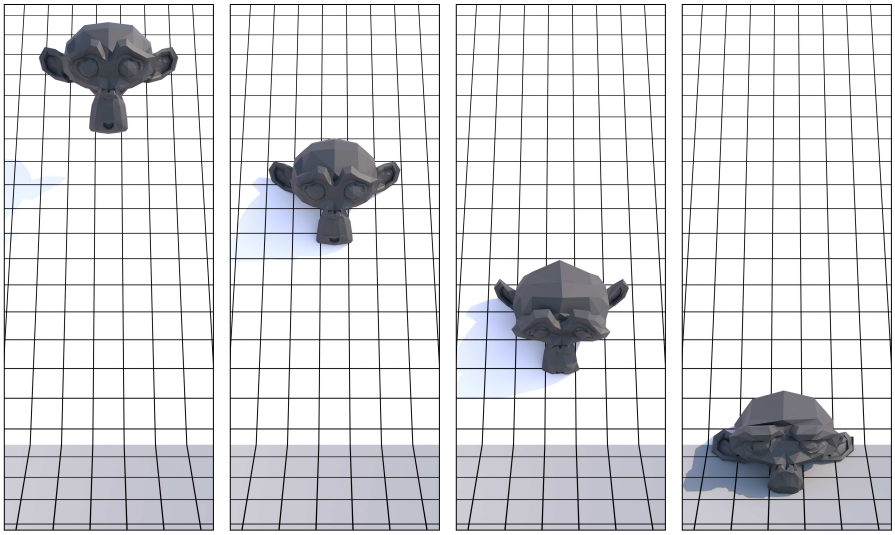

Fig. 29. Soft body deformation based on rigid body simulation of spheres with movement constraints

4.3.4 Results

Final Simulation

Returning to Kolumbo and the cone model created in Section 4.3.1, a grid of spheres can now be generated in place of the dynamic (collapsing) part of the cone as seen in Fig. 30. By tuning the simulation parameters, including the number of spheres on the grid, the constraints between them, the friction applied by the collision planes shown in Fig. 22 and the smoothing parameter of the skinning method, the results shown in Fig. 31 are achieved.

The simulation of Fig. 31, clearly demonstrates the phenomena we want to highlight. The two tsunamogenic sources are distinctly visualized, with one being the violent downward motion of the flank and the other being the exposed magmatic vent, leading to phreatomagmatic interactions. At the same time, both the curved compressional ridges and the exposed detachment surface are exhibited, exactly as expected from the modern day topology of the northwest flank of the Kolumbo crater (shown in Fig. 20).

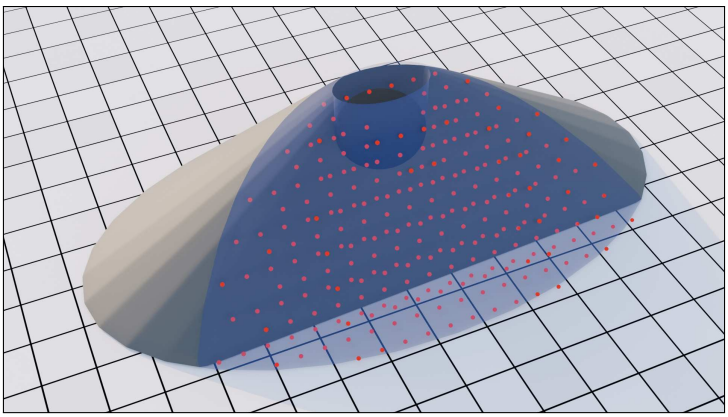

Fig. 30. Dynamic flank of volcanic cone (shown in blue) replaced with a grid of rigid spheres (shown in red)

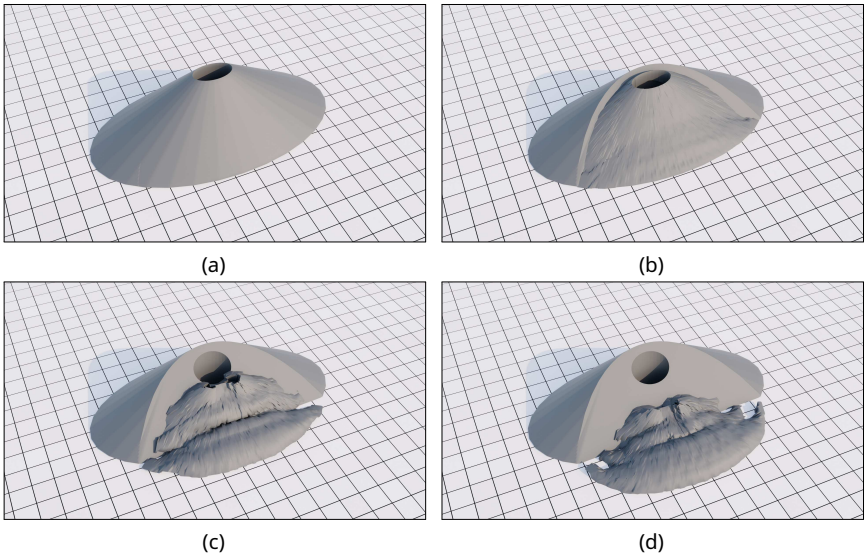

Fig. 31. Four frames from the final flank collapse simulation. The curved compressional ridges also present in the modern day Kolumbo crater are clearly visible

Realistic Rendering

For the creation of a more realistic visualization of this event now, only small modifications need to be made. First, to make the topology of the cone a bit more interesting, displacement can be added to the vertices using a pseudo-random texture. Proper procedurally generated materials can also be applied. Finally, to reintroduce the sea surface to the scene without greatly reducing visibility, the Glass BSDF described in Section 2.3.2 can be mixed with a transparency shader.

Smoke can be added to the vent to improve realism and keyframed to change characteristics as expected after the flank collapse. Similarly, a tsunami-like directed wave can be keyframed in after the collapse using the techniques described in Section 3.2. Using this method, the complete visualization shown in Fig. 32 can be created.

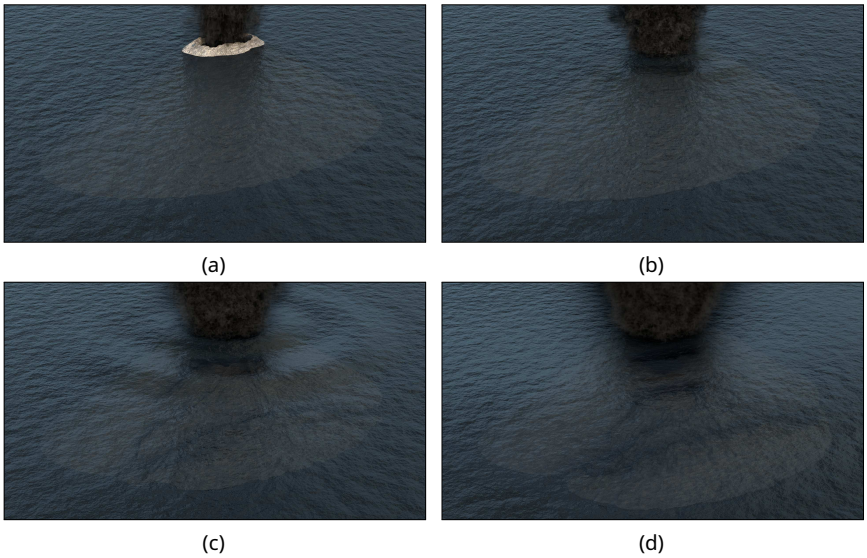

Fig. 32. Four frames from the final visualization of the Kolumbo flank collapse. The change to the eruption dynamics as well as the propagation of the directed tsunami caused by the collapse can be seen starting from frame (b)

Parameter Tuning

One of the limitations of the MSM, as described in Section 1.3.2, is the lack of direct correlation between the simulation parameters and the real material properties of the simulated object. This means that, in order to achieve a satisfactory result, like the one showcased in Fig. 31 and Fig. 32 significant manual tuning of the parameters is necessary. Some examples of the effects of different parameters are described bellow.

Starting from the number of spheres used to simulate the internal structure of the flank, a trade-off between accuracy and computational complexity must be evaluated. In addition, different phenomena appear at different scales. For example, the expected compressional ridges might not appear if the internal grid is tightly packed, as the spheres don't have a lot of freedom of movement. On the other hand, if the number of spheres is too low, especially around the perimeter of the flank, collisions will stop being properly detected. The total number of spheres used in Fig. 31 and visualized in Fig. 30 is 251.

The constraint limits set between neighboring spheres also have major impact on the final simulated dynamics. Tighter limits prevent the proper deformation of the flank, with the object essentially acting as a rigid body. On the other hand, looser limits allow the spheres to move freely without any interaction between them, creating a more fluid-like simulation. A middle ground between the two options is ideal for the simulation of the flank collapse.

The friction applied to the spheres by the two collision planes showcased in Fig. 22 affects the sliding speed of the flank and the total distance traveled. Finally, the smoothing parameter used in skinning, essentially controlling how many spheres are taken into account for each mesh vertex, prevents harsh edges and clumping around individual spheres. The optimal value for good smoothing and improved performance was found to be 3 spheres. A comparison of simulation runs with different parameter values is visualized in Fig. 33.

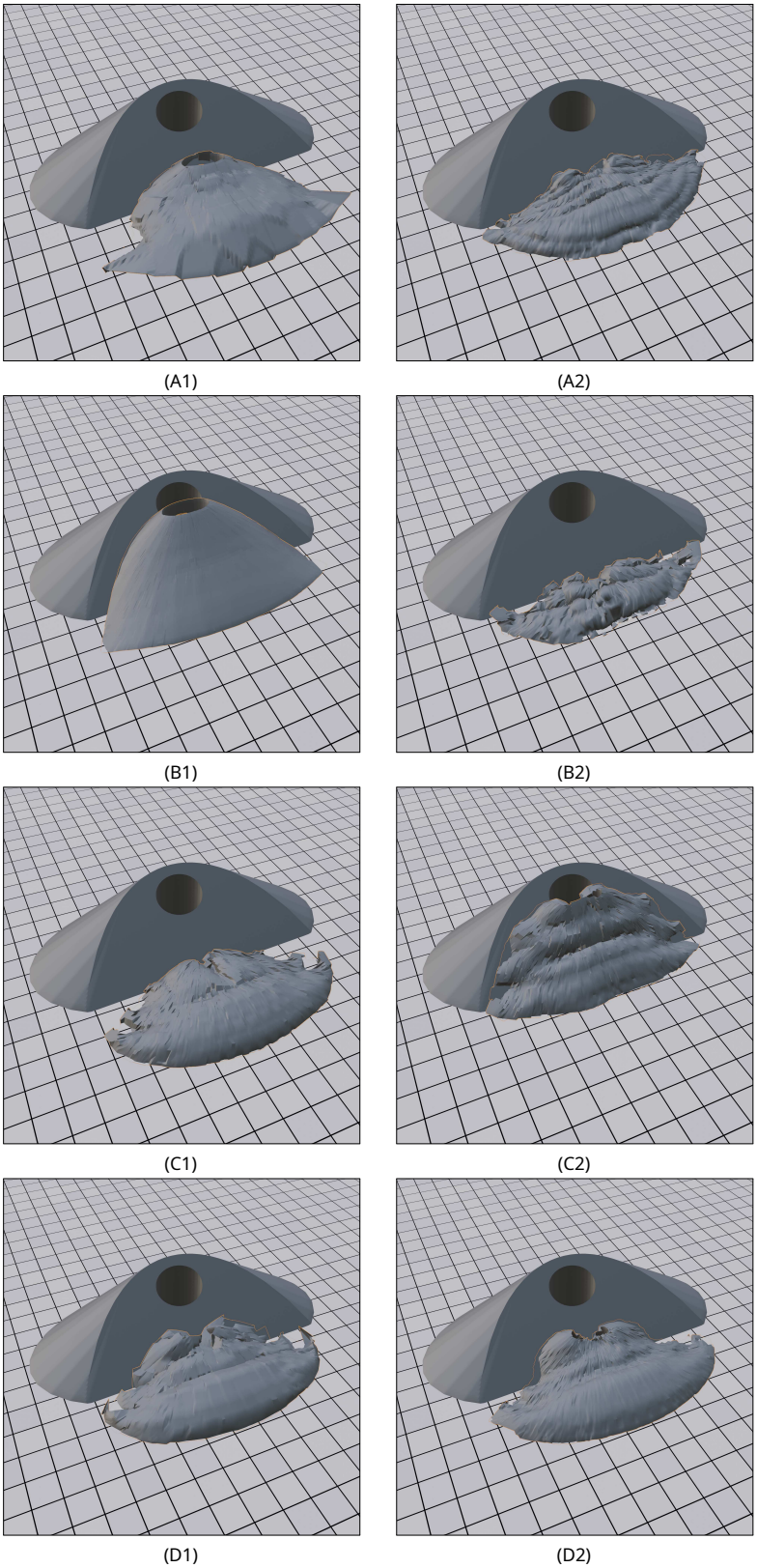

Fig. 33. Comparison of the effects of different parameters on the soft-body simulation (last frame of simulation shown). (A1) Small number of spheres (A2) Large number of spheres (B1) Tight constraints (B2) Loose constraints (C1) Low collision plane friction (C2) High collision plane friction (D1) Low smoothing (D2) High smoothing

5 Discussion and Conclusion

5.1 Overview of Results

hm2obj

In Section 2, during the island reconstruction process, a limitation was observed in the available tooling for generation of render-ready models from DEMs or heightmaps. In response, an automated command-line tool, named *hm2obj*, was developed for this procedure. Among other features, hm2obj streamlines the process of removing unwanted topology (e.g. the sea) without creating any artifacts on the produced mesh. Using this tool, an accurate mesh of 1650 CE Santorini was created (see Fig. 34a). This model was also combined with a 3D model of the northeastern seabed of Santorini, which was also generated using hm2obj and included the Kolumbo volcanic field.

Volcanic Plume

In Section 3, although multiple subaerial phenomena where explored, the most interesting advancement was made in the realistic visualization of volcanic plumes. This was achieved using a combination of a particle system for the large scale simulation of the plume dynamics, with a voxel-based approach for creating realistic smoke in their path. Using this layered method, different parameters and external forces can be trialed in real time to create the desired result, without sacrificing the realism of the final render (see Fig. 34b). The entire lifetime of the plume can also be animated using this method to showcase the propagation speed of ash in a given eruptive event.

Flank Collapse

Finally, in Section 4, while focusing on the submarine phenomena, the emphasis was placed on simulating the tsunamogenic collapse of the northwestern flank of Kolumbo during the 1650 CE eruption. This collapse was simulated and visualized using a modified version of the Mass-Spring Model (MSM), commonly used for the simulation of soft-body dynamics, built on top of the rigid body physics engine of Blender. Using this approach, an accurate representation of the most important aspects of this collapse was created (see Fig. 34c).

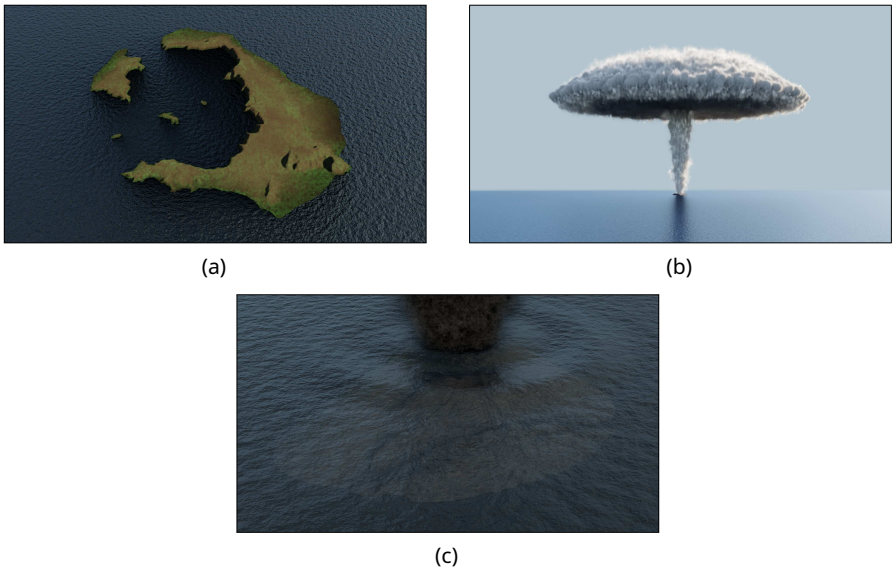

Fig. 34. Three highlighted results from this work. (a) 3D model of 1650 CE Santorini created using hm2obj (b) Volcanic plume render and (c) Simulation of flank collapse

5.2 Limitations

Summary

Although multiple volcanic phenomena where successfully simulated and visualized in this work, several limitations of the proposed methods must be acknowledged. Initially, the high computational cost of some methods, the lack of pre-existing tools, and the limited number of past research in this area posed some challenges, but these were eventually overcome. On the other hand, two more general issues arose throughout this work. The first one was the need for manual fine-tuning and iterative refinement of the different parameters for each method. The second, and possibly more important one, is the lack of user-friendliness, not only of the proposed solutions, but also of most existing CG tools for use directly by geologists.

Parameter Tuning

With realistic visualizations prioritized over accurate simulations, the need for extensive, manual fine-tuning of parameters based on expected results and empirical knowledge was unavoidable. This, however, limits the usefulness of the proposed methods in cases where fast (and ideally automatic) generation of visualizations is necessary. For example, even though these methods can be used for communication of future risks from volcanic activity in a given area, they are unfit for emergency situations where real-time data must be quickly visualized and provided to the public.

A clear example of this limitation is showcased in Fig. 33, where the effect of different parameters is compared for the flank collapse simulation. The goal in this case was to tune the parameters in such a way that the modern-day topology of the Kolumbo field was mimicked by the final step of the simulation. This goal, combined with the need for *realism* in the flank movement speed and behavior, cannot be easily formalized in such a way that automatic optimization techniques can be employed.

Accessibility and Usability

While the proposed methods demonstrate the potential of modern CG for the creation of complex realistic visualizations of volcanic phenomena, they also highlight the significant gap between fields like geology and CG. With terminology, data storage formats and tools being inherently different, bridging this gap would require substantial work coming from both sides.

As an example, focusing on the tool developed in Section 2 for converting heightmaps to render-ready models, significant changes would need to be made to accommodate its use directly by geologists. The reliance on a command line interface with strict input and output formats makes the tool less accessible to those with no prior programming knowledge. Ideally, the interface between GIS and CG software would need to be made entirely streamlined and automatic, enabling scientists to create realistic visualizations without requiring extensive technical expertise.

5.3 Future Directions

Complete Visualization of Single Eruption

Building on the findings and limitations discussed in this work, several avenues for future development can be identified. First, an application of the explored methods for the creation of a complete visualization of a specific eruption (e.g. the 1650 CE eruption of Kolumbo), would be beneficial for demonstrating the practical effectiveness of these visualizations in communicating complex geological events. Extensive tuning of the different method parameters as explained in Section 5.2 would be necessary for this cause, along with complete implementations of other methods for secondary phenomena, for example as described in Section 3.3.

Faster Parameter Tuning

Use of automation techniques, including ML methods, for tuning the parameters of the different methods would also be a significant advancement. For example the automatic generation of masks based on satellite imagery, as described in Section 2, using machine vision techniques could be explored. Faster parameter tuning could also be achieved with better understanding of the parameters themselves and their relation to the true geological properties of the simulated phenomena. For example, the parameters of the proposed internal model for soft bodies, based on the MSM, described in Section 4.3.3 could be associated with the inherent material properties of the simulated object.

Usability

Finally, in order to bridge the interdisciplinary gap described in Section 5.2, extensive work could be put into making the proposed methods and developed tools easier to use. For example, most methods described, including the heightmap to render-ready 3D model tool developed, could be directly implemented as plugins to modern CG software like Blender. This way, by providing a robust GUI, the described solutions could be easily utilized by geologists and other scientists without requiring extensive programming or other technical knowledge.

5.4 Final Thoughts

Reflection

Reflecting on the primary objectives of this work outlined in Section 1, although significant progress was made in visualizing complex volcanic phenomena using modern CG techniques, the challenges faced highlight the increased need for better tooling and greater interdisciplinary cooperation. Thus, considerable work remains to be done by engineers and scientists to allow for quicker and simpler production of such visualizations.

Despite the technological advancements available today, we have yet to fully utilize their potential across different scientific fields. With the rapid pace of innovation, it is crucial to dedicate resources to bridging this gap. Visualizations, like the ones showcased in Section 5.1, could have a significant impact on science communication efforts, allowing for better decision-making by policymakers and improved preparedness by the public. At the same, they could provide scientists with better insights into the visualized phenomena, pushing the boundaries of scientific research.

References

[1] "Science Communication", in *The Hands-On Guide For Science Communicators: A Step-By-Step Approach to Public Outreach*, L. L. Christensen, Ed., New York, NY: Springer, 2007, pp. 3–6, ISBN: 978-0-387-49960-4. DOI: 10.1007/978-0-387-49960-4_1. [Online]. Available: https://doi.org/10.1007/978-0-387-49960-4_1.

[2] M. Westerlund, "The Emergence of Deepfake Technology: A Review", *Technology Innovation Management Review*, vol. 9, no. 11, pp. 39–52, Jan. 1, 2019, ISSN: 19270321. DOI: 10.22215/timreview/1282. [Online]. Available: https://timreview.ca/article/1282.

[3] T. F. Blauth, O. J. Gstrein, and A. Zwitter, "Artificial Intelligence Crime: An Overview of Malicious Use and Abuse of AI", *IEEE Access*, vol. 10, pp. 77 110–77 122, 2022, ISSN: 2169-3536. DOI: 10.1109/ACCESS.2022.3191790. [Online]. Available: https://ieeexplore.ieee.org/document/9831441/.

[4] B. Millet, A. P. Carter, K. Broad, A. Cairo, S. D. Evans, and S. J. Majumdar, "Hurricane Risk Communication: Visualization and Behavioral Science Concepts", *Weather, Climate, and Society*, vol. 12, no. 2, pp. 193–211, Apr. 1, 2020, ISSN: 1948-8327, 1948-8335. DOI: 10.1175/WCAS-D-19-0011.1. [Online]. Available: https://journals.ametsoc.org/view/journals/wcas/12/2/wcas-d-19-0011.1.xml.

[5] M. D. Gerst, M. A. Kenney, A. E. Baer, *et al.*, "Using Visualization Science to Improve Expert and Public Understanding of Probabilistic Temperature and Precipitation Outlooks", *Weather, Climate, and Society*, vol. 12, no. 1, pp. 117–133, Jan. 1, 2020, ISSN: 1948-8327, 1948-8335. DOI: 10.1175/WCAS-D-18-0094.1. [Online]. Available: https://journals.ametsoc.org/view/journals/wcas/12/1/wcas-d-18-0094.1.xml.

[6] K. Shatri and K. Buza, "The Use of Visualization in Teaching and Learning Process for Developing Critical Thinking of Students", *European Journal of Social Sciences Education and Research*, vol. 9, no. 1, p. 71, Jan. 21, 2017, ISSN: 2312-8429, 2411-9563. DOI: 10.26417/ejser.v9i1.p71-74. [Online]. Available: https://revistia.com/index.php/ejser/article/view/6470.

[7] D. Salomon, *The Computer Graphics Manual*. Springer Science & Business Media, Sep. 18, 2011, 1559 pp., ISBN: 978-0-85729-886-7. Google Books: DX4YstV76c4C.

[8] A. Lehmuskallio, J. Häkkinen, and J. Seppänen, "Photorealistic computer-generated images are difficult to distinguish from digital photographs: A case study with professional photographers and photo-editors", *Visual Communication*, vol. 18, no. 4, pp. 427–451, Nov. 1, 2019, ISSN: 1470-3572. DOI: 10.1177/1470357218759809. [Online]. Available: https://doi.org/10.1177/1470357218759809.

[9] P. Farabollini, F. R. Lugeri, B. Aldighieri, and V. Amadio, "The Role of Earth Science and Landscape Approach in the Ethic Geology: Communication and Divulgation for the Prevention and Reduction of Geological Hazard", in *Engineering Geology for Society and Territory - Volume 7*, G. Lollino, M. Arattano, M. Giardino, R. Oliveira, and S. Peppoloni, Eds., Cham: Springer International Publishing, 2014, pp. 115–120, ISBN: 978-3-319-09303-1. DOI: 10.1007/978-3-319-09303-1_22.

[10] A. Katsigera, P. Nomikou, and SANTORY Team, "Addressing the hazard risks of Kolumbo submarine volcano (Santorini, Greece)", in *Proceedings of the International Conference on Humanitarian Crisis Management (KRISIS 2023)*, Thessaloniki, Greece, Oct. 15, 2023. [Online]. Available: https://www.ihu.gr/ucips/krisis#proceedings.

[11] Hellenic Statistical Authority (ELSTAT). "Population-Housing Census". (2021), [Online]. Available: https://www.statistics.gr/en/2021-census-pop-hous.

[12] T. H. Druitt, F. W. McCoy, and G. E. Vougioukalakis, "The Late Bronze Age Eruption of Santorini Volcano and Its Impact on the Ancient Mediterranean World", *Elements*, vol. 15, no. 3, pp. 185–190, Jun. 1, 2019, ISSN: 1811-5217, 1811-5209. DOI: 10.2138/gselements.15.3.185. [Online]. Available: https://pubs.geoscienceworld.org/msa/elements/article/15/3/185/571624/The-Late-Bronze-Age-Eruption-of-Santorini-Volcano.

[13] W. L. Friedrich, *Fire in the Sea: The Santorini Volcano : Natural History and the Legend of Atlantis*. Cambridge University Press, 2000, 258 pp., ISBN: 978-0-521-65290-2. Google Books: xHtuQgAACAAJ.

[14] D. Karátson, R. Gertisser, T. Telbisz, *et al.*, "Towards reconstruction of the lost Late Bronze Age intra-caldera island of Santorini, Greece", *Scientific Reports*, vol. 8, no. 1, p. 7026, May 4, 2018, ISSN: 2045-2322. DOI: 10.1038/s41598-018-25301-2. [Online]. Available: https://www.nature.com/articles/s41598-018-25301-2.

[15] P. Nomikou, S. Carey, D. Papanikolaou, *et al.*, "Submarine Volcanoes of the Kolumbo volcanic zone NE of Santorini Caldera, Greece", *Global and Planetary Change*, vol. s 90–91, pp. 135–151, Jun. 1, 2012. DOI: 10.1016/j.gloplacha.2012.01.001.

[16] M. D. Hannington, "RV POSEIDON Fahrtbericht / Cruise Report POS510 - ANYDROS: Rifting and Hydrothermal Activity in the Cyclades Back-arc Basin, Catania (Italy) – Heraklion (Greece) 06.03.-29.03.2017", GEOMAR Helmholtz-Zentrum für Ozeanforschung, Kiel, Germany, Report, 2018, 56 + Appendix. DOI: 10.3289/geomar_rep_ns_43_2018. [Online]. Available: https://oceanrep.geomar.de/id/eprint/44466/.

[17] K. Cantner, S. Carey, and P. Nomikou, "Integrated volcanologic and petrologic analysis of the 1650 AD eruption of Kolumbo submarine volcano, Greece", *Journal of Volcanology and Geothermal Research*, vol. 269, pp. 28–43, Jan. 1, 2014, ISSN: 0377-0273. DOI: 10.1016/j.jvolgeores.2013.10.004. [Online]. Available: https://www.sciencedirect.com/science/article/pii/S0377027313002953.

[18] F. Fouqué, *Santorin et ses éruptions*. G. Masson, 1879, 690 pp. Google Books: fvgwAQAAMAAJ.

[19] J. Karstens, G. J. Crutchley, T. H. Hansteen, *et al.*, "Cascading events during the 1650 tsunamigenic eruption of Kolumbo volcano", *Nature Communications*, vol. 14, no. 1, p. 6606, 1 Oct. 26, 2023, ISSN: 2041-1723. DOI: 10.1038/s41467-023-42261-y. [Online]. Available: https://www.nature.com/articles/s41467-023-42261-y.

[20] P. Nomikou, M. M. Parks, D. Papanikolaou, *et al.*, "The emergence and growth of a submarine volcano: The Kameni islands, Santorini (Greece)", *GeoResJ*, vol. 1–2, pp. 8–18, Mar. 1, 2014, ISSN: 2214-2428. DOI: 10.1016/j.grj.2014.02.002. [Online]. Available: https://www.sciencedirect.com/science/article/pii/S2214242814000047.

[21] A. G. Whitham and R. S. J. Sparks, "Pumice", *Bulletin of Volcanology*, vol. 48, no. 4, pp. 209–223, Aug. 1, 1986, ISSN: 1432-0819. DOI: 10.1007/BF01087675. [Online]. Available: https://doi.org/10.1007/BF01087675.

[22] I. V. Kerlow, *The Art of 3D: Computer Animation and Effects*. John Wiley & Sons, 2004, 470 pp., ISBN: 978-0-471-43036-0.

[23] T. Schenk, "Introduction to Photogrammetry", *The Ohio State University, Columbus*, vol. 106, no. 1, 2005.

[24] A. S. Glassner, *An Introduction to Ray Tracing*. Morgan Kaufmann, Jan. 28, 1989, 364 pp., ISBN: 978-0-12-286160-4. Google Books: YPblYyLqBM4C.

[25] Blender Foundation, *Blender*, version 4.1. [Online]. Available: https://www.blender.org/.

[26] R. Fedkiw, "Simulating Natural Phenomena for Computer Graphics", in *Geometric Level Set Methods in Imaging, Vision, and Graphics*, S. Osher and N. Paragios, Eds., New York, NY: Springer, 2003, pp. 461–479, ISBN: 978-0-387-21810-6. DOI: 10.1007/0-387-21810-6_24. [Online]. Available: https://doi.org/10.1007/0-387-21810-6_24.

[27] I. Millington, *Game Physics Engine Development*. Boca Raton: CRC Press, Apr. 21, 2014, 480 pp., ISBN: 978-0-429-17855-9. DOI: 10.1201/9781482267327.

[28] C. D. Freeman, E. Frey, A. Raichuk, S. Girgin, I. Mordatch, and O. Bachem. "Brax – A Differentiable Physics Engine for Large Scale Rigid Body Simulation". arXiv: 2106.13281 [cs]. (Jun. 24, 2021), [Online]. Available: http://arxiv.org/abs/2106.13281, pre-published.

[29] R. Weller, "A Brief Overview of Collision Detection", in *New Geometric Data Structures for Collision Detection and Haptics*, R. Weller, Ed., Heidelberg: Springer International Publishing, 2013, pp. 9–46, ISBN: 978-3-319-01020-5. DOI: 10.1007/978-3-319-01020-5_2. [Online]. Available: https://doi.org/10.1007/978-3-319-01020-5_2.

[30] R. Bridson, *Fluid Simulation for Computer Graphics*, 2nd ed. New York: A K Peters/CRC Press, Sep. 25, 2015, 276 pp., ISBN: 978-1-315-26600-8. DOI: 10.1201/9781315266008.

[31] R. Vinuesa and S. L. Brunton, "Enhancing Computational Fluid Dynamics with Machine Learning", *Nature Computational Science*, vol. 2, no. 6, pp. 358–366, Jun. 27, 2022, ISSN: 2662-8457. DOI: 10.1038/s43588-022-00264-7. arXiv: 2110.02085 [physics]. [Online]. Available: http://arxiv.org/abs/2110.02085.

[32] A. Nealen, M. Müller, R. Keiser, E. Boxerman, and M. Carlson, "Physically Based Deformable Models in Computer Graphics", *Computer Graphics Forum*, vol. 25, no. 4, pp. 809–836, 2006, ISSN: 1467-8659. DOI: 10.1111/j.1467-8659.2006.01000.x. [Online]. Available: https://onlinelibrary.wiley.com/doi/abs/10.1111/j.1467-8659.2006.01000.x.

[33] H. Va, M.-H. Choi, and M. Hong, "Real-Time Surface-Based Volume Constraints on Mass-Spring Model in Unity3D", *IEEE Access*, vol. 11, pp. 17 857–17 869, 2023, ISSN: 2169-3536. DOI: 10.1109/ACCESS.2023.3245130. [Online]. Available: https://ieeexplore.ieee.org/abstract/document/10044641.

[34] D. Koschier, J. Bender, B. Solenthaler, and M. Teschner, "A Survey on SPH Methods in Computer Graphics", *Computer Graphics Forum*, vol. 41, no. 2, pp. 737–760, 2022, ISSN: 1467-8659. DOI: 10.1111/cgf.14508. [Online]. Available: https://onlinelibrary.wiley.com/doi/abs/10.1111/cgf.14508.

[35] S. Whitmeyer, J. Nicoletti, and D. De Paor, "The digital revolution in geologic mapping", *GSA Today*, pp. 4–10, Apr. 2010, ISSN: 10525173. DOI: 10.1130/GSATG70A.1. [Online]. Available: http://www.geosociety.org/gsatoday/archive/20/4/abstract/i1052-5173-20-4-4.htm.

[36] T. D. Seers, A. Sheharyar, S. Tavani, and A. Corradetti, "Virtual outcrop geology comes of age: The application of consumer-grade virtual reality hardware and software to digital outcrop data analysis", *Computers & Geosciences*, vol. 159, p. 105 006, Feb. 1, 2022, ISSN: 0098-3004. DOI: 10.1016/j.cageo.2021.105006. [Online]. Available: https://www.sciencedirect.com/science/article/pii/S0098300421002892.

[37] G. Pehlivanides, K. Monastiridis, A. Tourtas, *et al.*, "The VIRTUALDiver Project. Making Greece's Underwater Cultural Heritage Accessible to the Public", *Applied Sciences*, vol. 10, no. 22, p. 8172, 22 Jan. 2020, ISSN: 2076-3417. DOI: 10.3390/app10228172. [Online]. Available: https://www.mdpi.com/2076-3417/10/22/8172.

[38] S. Marras and K. T. Mandli, "Modeling and Simulation of Tsunami Impact: A Short Review of Recent Advances and Future Challenges", *Geosciences*, vol. 11, no. 1, p. 5, 1 Jan. 2021, ISSN: 2076-3263. DOI: 10.3390/geosciences11010005. [Online]. Available: https://www.mdpi.com/2076-3263/11/1/5.

[39] A. Giannakidis, G. Giakoumidakis, and K. Mania, "3D photorealistic scientific visualization of tsunami waves and sea level rise", in *2014 IEEE International Conference on Imaging Systems and Techniques (IST) Proceedings*, Oct. 2014, pp. 167–172. DOI: 10.1109/IST.2014.6958467. [Online]. Available: https://ieeexplore.ieee.org/abstract/document/6958467.

[40] P. Luo, M. Luo, F. Li, *et al.*, "Urban flood numerical simulation: Research, methods and future perspectives", *Environmental Modelling & Software*, vol. 156, p. 105 478, Oct. 1, 2022, ISSN: 1364-8152. DOI: 10.1016/j.envsoft.2022.105478. [Online]. Available: https://www.sciencedirect.com/science/article/pii/S1364815222001827.

[41] B. Lütjens, B. Leshchinskiy, C. Requena-Mesa, *et al.* "Physically-Consistent Generative Adversarial Networks for Coastal Flood Visualization". arXiv: 2104.04785 [cs, eess]. (Feb. 21, 2023), [Online]. Available: http://arxiv.org/abs/2104.04785, pre-published.

[42] D. McCallen, A. Petersson, A. Rodgers, *et al.*, "EQSIM—A multidisciplinary framework for fault-to-structure earthquake simulations on exascale computers part I: Computational models and workflow", *Earthquake Spectra*, vol. 37, no. 2, pp. 707–735, May 1, 2021, ISSN: 8755-2930. DOI: 10.1177/8755293020970982. [Online]. Available: https://doi.org/10.1177/8755293020970982.

[43] Z. Xu, Y. Wu, X. Lu, and X. Jin, "Photo-realistic visualization of seismic dynamic responses of urban building clusters based on oblique aerial photography", *Advanced Engineering Informatics*, vol. 43, p. 101 025, Jan. 1, 2020, ISSN: 1474-0346. DOI: 10.1016/j.aei.2019.101025. [Online]. Available: https://www.sciencedirect.com/science/article/pii/S1474034619305981.

[44] W.-H. Yuan, K. Liu, W. Zhang, B. Dai, and Y. Wang, "Dynamic modeling of large deformation slope failure using smoothed particle finite element method", *Landslides*, vol. 17, no. 7, pp. 1591–1603, Jul. 1, 2020, ISSN: 1612-5118. DOI: 10.1007/s10346-020-01375-w. [Online]. Available: https://doi.org/10.1007/s10346-020-01375-w.

[45] G. H. Alene, H. Vicari, S. Irshad, A. Perkis, O. Bruland, and V. Thakur, "Realistic visualization of debris flow type landslides through virtual reality", *Landslides*, vol. 20, no. 1, pp. 13–23, Jan. 1, 2023, ISSN: 1612-5118. DOI: 10.1007/s10346-022-01948-x. [Online]. Available: https://doi.org/10.1007/s10346-022-01948-x.

[46] M. Cerminara, T. Esposti Ongaro, and A. Neri, "Large Eddy Simulation of gas–particle kinematic decoupling and turbulent entrainment in volcanic plumes", *Journal of Volcanology and Geothermal Research*, Numerical Models of Volcanic Eruption Plumes: Inter-Comparison and Sensitivity, vol. 326, pp. 143–171, Oct. 15, 2016, ISSN: 0377-0273. DOI: 10.1016/j.jvolgeores.2016.06.018. [Online]. Available: https://www.sciencedirect.com/science/article/pii/S0377027316301688.

[47] Z. Cao, M. Bursik, Q. Yang, and A. Patra, "Simulating the Transport and Dispersal of Volcanic Ash Clouds With Initial Conditions Created by a 3D Plume Model", *Frontiers in Earth Science*, vol. 9, Sep. 23, 2021, ISSN: 2296-6463. DOI: 10.3389/feart.2021.704797. [Online]. Available: https://www.frontiersin.org/articles/10.3389/feart.2021.704797.

[48] J. de Leeuw, A. Schmidt, C. S. Witham, *et al.*, "The 2019 Raikoke volcanic eruption – Part 1: Dispersion model simulations and satellite retrievals of volcanic sulfur dioxide", *Atmospheric Chemistry and Physics*, vol. 21, no. 14, pp. 10 851–10 879, Jul. 19, 2021, ISSN: 1680-7316. DOI: 10.5194/acp-21-10851-2021. [Online]. Available: https://acp.copernicus.org/articles/21/10851/2021/.

[49] J. Youn and T. Kim, "3D VISUALIZATION OF VOLCANIC ASH DISPERSION PREDICTION WITH SPATIAL INFORMATION OPEN PLATFORM IN KOREA", *The International Archives of the Photogrammetry, Remote Sensing and Spatial Information Sciences*, vol. XLI-B8, pp. 185–190, Jun. 22, 2016, ISSN: 1682-1750. DOI: 10.5194/isprs-archives-XLI-B8-185-2016. [Online]. Available: https://isprs-archives.copernicus.org/articles/XLI-B8/185/2016/.

[50] B. Cordonnier, E. Lev, and F. Garel, "Benchmarking lava-flow models", *Geological Society, London, Special Publications*, vol. 426, no. 1, pp. 425–445, Jan. 2016, ISSN: 0305-8719, 2041-4927. DOI: 10.1144/SP426.7. [Online]. Available: https://www.lyellcollection.org/doi/10.1144/SP426.7.

[51] A. Rodriguez-Gonzalez, M. Aulinas, S. Mossoux, *et al.*, "Comparison of real and simulated lava flows in the Holocene volcanism of Gran Canaria (Canary Islands, Spain) with Q-LavHA: Contribution to volcanic hazard management", *Natural Hazards*, vol. 107, no. 2, pp. 1785–1819, Jun. 1, 2021, ISSN: 1573-0840. DOI: 10.1007/s11069-021-04660-6. [Online]. Available: https://doi.org/10.1007/s11069-021-04660-6.

[52] G. B. M. Pedersen, M. A. Pfeffer, S. Barsotti, *et al.*, "Lava flow hazard modelling during the 2021 Fagradalsfjall eruption, Iceland: Applications of MrLavaLoba", *Natural Hazards and Earth System Sciences Discussions*, pp. 1–38, Jun. 23, 2022. DOI: 10.5194/nhess-2022-166. [Online]. Available: https://nhess.copernicus.org/preprints/nhess-2022-166/.

[53] R. deGraffenried, J. Hammer, H. Dietterich, R. Perroy, M. Patrick, and T. Shea, "Evaluating lava flow propagation models with a case study from the 2018 eruption of Kīlauea Volcano, Hawai'i", *Bulletin of Volcanology*, vol. 83, no. 11, p. 65, Oct. 5, 2021, ISSN: 1432-0819. DOI: 10.1007/s00445-021-01492-x. [Online]. Available: https://doi.org/10.1007/s00445-021-01492-x.

[54] G. H. Alene, S. Irshad, A. Moraru, *et al.*, "Virtual reality visualization of geophysical flows: A framework", *Environmental Modelling & Software*, vol. 177, p. 106 063, Jun. 1, 2024, ISSN: 1364-8152. DOI: 10.1016/j.envsoft.2024.106063. [Online]. Available: https://www.sciencedirect.com/science/article/pii/S1364815224001245.

[55] A. Amores, S. Monserrat, M. Marcos, *et al.*, "Numerical Simulation of Atmospheric Lamb Waves Generated by the 2022 Hunga-Tonga Volcanic Eruption", *Geophysical Research Letters*, vol. 49, no. 6, e2022GL098240, 2022, ISSN: 1944-8007. DOI: 10.1029/2022GL098240. [Online]. Available: https://onlinelibrary.wiley.com/doi/abs/10.1029/2022GL098240.

[56] A. Aravena, M. d. M. Vitturi, R. Cioni, and A. Neri, "Physical constraints for effective magma-water interaction along volcanic conduits during silicic explosive eruptions", *Geology*, vol. 46, no. 10, pp. 867–870, Sep. 7, 2018, ISSN: 0091-7613. DOI: 10.1130/G45065.1. [Online]. Available: https://doi.org/10.1130/G45065.1.

[57] A. Asgary, C. Bonadonna, and C. Frischknecht, "Simulation and Visualization of Volcanic Phenomena Using Microsoft Hololens: Case of Vulcano Island (Italy)", *IEEE Transactions on Engineering Management*, vol. 67, no. 3, pp. 545–553, Aug. 2020, ISSN: 1558-0040. DOI: 10.1109/TEM.2019.2932291. [Online]. Available: https://ieeexplore.ieee.org/abstract/document/8823985.

[58] M. Lütjens, T. P. Kersten, B. Dorschel, and F. Tschirschwitz, "Virtual Reality in Cartography: Immersive 3D Visualization of the Arctic Clyde Inlet (Canada) Using Digital Elevation Models and Bathymetric Data", *Multimodal Technologies and Interaction*, vol. 3, no. 1, p. 9, 1 Mar. 2019, ISSN: 2414-4088. DOI: 10.3390/mti3010009. [Online]. Available: https://www.mdpi.com/2414-4088/3/1/9.

[59] A. El Saer, C. Stentoumis, I. Kalisperakis, and P. Nomikou, "DEVELOPING A STRATEGY FOR PRECISE 3D MODELLING OF LARGE-SCALE SCENES FOR VR", *The International Archives of the Photogrammetry, Remote Sensing and Spatial Information Sciences*, vol. XLIII-B4-2020, pp. 567–574, Aug. 25, 2020, ISSN: 1682-1750. DOI: 10.5194/isprs-archives-XLIII-B4-2020-567-2020. [Online]. Available: https://isprs-archives.copernicus.org/articles/XLIII-B4-2020/567/2020/.

[60] A. Balasubramanian, *DIGITAL ELEVATION MODEL (DEM) IN GIS*. Sep. 3, 2017. DOI: 10.13140/RG.2.2.23976.47369.

[61] The Inkscape Team, *Inkscape*, version 1.3.2, 2023. [Online]. Available: https://inkscape.org/.

[62] Python Software Foundation, *Python*, version 3.11. [Online]. Available: https://www.python.org/.

[63] Blender Documentation Team. "Blender 4.1 Manual". (2024), [Online]. Available: https://docs.blender.org/manual/en/4.1/index.html.

[64] S. Worley, "A cellular texture basis function", in *Proceedings of the 23rd Annual Conference on Computer Graphics and Interactive Techniques*, ser. SIGGRAPH '96, New York, NY, USA: Association for Computing Machinery, Aug. 1, 1996, pp. 291–294, ISBN: 978-0-89791-746-9. DOI: 10.1145/237170.237267. [Online]. Available: https://dl.acm.org/doi/10.1145/237170.237267.

[65] T. Nishita, T. Sirai, K. Tadamura, and E. Nakamae, "Display of the earth taking into account atmospheric scattering", in *Proceedings of the 20th Annual Conference on Computer Graphics and Interactive Techniques*, Anaheim CA: ACM, Sep. 1993, pp. 175–182, ISBN: 978-0-89791-601-1. DOI: 10.1145/166117.166140. [Online]. Available: https://dl.acm.org/doi/10.1145/166117.166140.

[66] J. P. Terry, J. Goff, N. Winspear, V. P. Bongolan, and S. Fisher, "Tonga volcanic eruption and tsunami, January 2022: Globally the most significant opportunity to observe an explosive and tsunamigenic submarine eruption since AD 1883 Krakatau", *Geoscience Letters*, vol. 9, no. 1, p. 24, Jun. 28, 2022, ISSN: 2196-4092. DOI: 10.1186/s40562-022-00232-z. [Online]. Available: https://doi.org/10.1186/s40562-022-00232-z.

[67] S. Carey and M. Bursik, "Volcanic Plumes", in *The Encyclopedia of Volcanoes*, Elsevier, 2015, pp. 571–585, ISBN: 978-0-12-385938-9. DOI: 10.1016/B978-0-12-385938-9.00032-8. [Online]. Available: https://linkinghub.elsevier.com/retrieve/pii/B9780123859389000328.

[68] M. Lastic, D. Rohmer, G. Cordonnier, C. Jaupart, F. Neyret, and M.-P. Cani, "Interactive simulation of plume and pyroclastic volcanic ejections", *Proceedings of the ACM on Computer Graphics and Interactive Techniques*, vol. 5, no. 1, 4:1–4:15, May 4, 2022. DOI: 10.1145/3522609. [Online]. Available: https://dl.acm.org/doi/10.1145/3522609.

[69] A. Kaufman and K. Mueller, "Overview of Volume Rendering", in *Visualization Handbook*, Elsevier, 2005, pp. 127–174, ISBN: 978-0-12-387582-2. DOI: 10.1016/B978-012387582-2/50009-5. [Online]. Available: https://linkinghub.elsevier.com/retrieve/pii/B9780123875822500095.

[70] K. Museth, J. Lait, J. Johanson, *et al.*, "OpenVDB: An open-source data structure and toolkit for high-resolution volumes", in *ACM SIGGRAPH 2013 Courses*, ser. SIGGRAPH '13, New York, NY, USA: Association for Computing Machinery, Jul. 21, 2013, p. 1, ISBN: 978-1-4503-2339-0. DOI: 10.1145/2504435.2504454. [Online]. Available: https://dl.acm.org/doi/10.1145/2504435.2504454.

[71] K. Museth, "NanoVDB: A GPU-Friendly and Portable VDB Data Structure For Real-Time Rendering And Simulation", in *ACM SIGGRAPH 2021 Talks*, ser. SIGGRAPH '21, New York, NY, USA: Association for Computing Machinery, Aug. 6, 2021, pp. 1–2, ISBN: 978-1-4503-8373-8. DOI: 10.1145/3450623.3464653. [Online]. Available: https://dl.acm.org/doi/10.1145/3450623.3464653.

[72] Tonga Geological Services, director, *Hunga Volcano Eruption captured at 11:55am 30th December 2021*, Dec. 31, 2021. [Online]. Available: https://www.youtube.com/watch?v=CXZNlnuDnHg.

[73] R. Paris, "Source mechanisms of volcanic tsunamis", *Philosophical Transactions of the Royal Society A: Mathematical, Physical and Engineering Sciences*, vol. 373, no. 2053, p. 20140380, Oct. 28, 2015, ISSN: 1364-503X, 1471-2962. DOI: 10.1098/rsta.2014.0380. [Online]. Available: https://royalsocietypublishing.org/doi/10.1098/rsta.2014.0380.

[74] K. Kelfoun and S. V. Vargas, "VolcFlow capabilities and potential development for the simulation of lava flows", *Geological Society, London, Special Publications*, vol. 426, no. 1, pp. 337–343, Jan. 2016. DOI: 10.1144/SP426.8. [Online]. Available: https://www.lyellcollection.org/doi/abs/10.1144/sp426.8.

[75] A. Zanutta, A. Lambertini, and L. Vittuari, "UAV Photogrammetry and Ground Surveys as a Mapping Tool for Quickly Monitoring Shoreline and Beach Changes", *Journal of Marine Science and Engineering*, vol. 8, no. 1, p. 52, Jan. 18, 2020, ISSN: 2077-1312. DOI: 10.3390/jmse8010052. [Online]. Available: https://www.mdpi.com/2077-1312/8/1/52.

[76] P. J. Lynett, "Effect of a Shallow Water Obstruction on Long Wave Runup and Overland Flow Velocity", *Journal of Waterway, Port, Coastal, and Ocean Engineering*, vol. 133, no. 6, pp. 455–462, Nov. 1, 2007, ISSN: 0733-950X. DOI: 10.1061/(ASCE)0733-950X(2007)133:6(455). [Online]. Available: https://ascelibrary.org/doi/10.1061/%28ASCE%290733-950X%282007%29133%3A6%28455%29.

[77] D. P. Hill, F. Pollitz, and C. Newhall, "Earthquake–Volcano Interactions", *Physics Today*, vol. 55, no. 11, pp. 41–47, Nov. 1, 2002, ISSN: 0031-9228, 1945-0699. DOI: 10.1063/1.1535006. [Online]. Available: https://pubs.aip.org/physicstoday/article/55/11/41/443433/Earthquake-Volcano-InteractionsNew-measurements.

[78] R. Sinha, A. Sapre, A. Patil, A. Singhvi, M. Sathe, and V. Rathi, "Earthquake Disaster Simulation in Immersive 3D Environment",

[79] C. Cimarelli and K. Genareau, "A review of volcanic electrification of the atmosphere and volcanic lightning", *Journal of Volcanology and Geothermal Research*, vol. 422, p. 107 449, Feb. 1, 2022, ISSN: 0377-0273. DOI: 10.1016/j.jvolgeores.2021.107449. [Online]. Available: https://www.sciencedirect.com/science/article/pii/S037702732100278X.

[80] S. A. Behnke and S. R. McNutt, "Using lightning observations as a volcanic eruption monitoring tool", *Bulletin of Volcanology*, vol. 76, no. 8, p. 847, Jul. 27, 2014, ISSN: 1432-0819. DOI: 10.1007/s00445-014-0847-1. [Online]. Available: https://doi.org/10.1007/s00445-014-0847-1.

[81] S. R. McNutt and E. R. Williams, "Volcanic lightning: Global observations and constraints on source mechanisms", *Bulletin of Volcanology*, vol. 72, no. 10, pp. 1153–1167, Dec. 1, 2010, ISSN: 1432-0819. DOI: 10.1007/s00445-010-0393-4. [Online]. Available: https://doi.org/10.1007/s00445-010-0393-4.

[82] T. Kim and M. C. Lin, "Fast Animation of Lightning Using an Adaptive Mesh", *IEEE Transactions on Visualization and Computer Graphics*, vol. 13, no. 2, pp. 390–402, Mar. 2007, ISSN: 1941-0506. DOI: 10.1109/TVCG.2007.38. [Online]. Available: https://ieeexplore.ieee.org/abstract/document/4069246.

[83] Y. Dobashi, T. Yamamoto, and T. Nishita, "Efficient rendering of lightning taking into account scattering effects due to clouds and atmospheric particles", in *Proceedings Ninth Pacific Conference on Computer Graphics and Applications. Pacific Graphics 2001*, Oct. 2001, pp. 390–399. DOI: 10.1109/PCCGA.2001.962896. [Online]. Available: https://ieeexplore.ieee.org/abstract/document/962896.

[84] S. Liu, S. Gao, and S. Xu, "Animating explosion with exploding sound and rigid-body sound", *Computer Animation and Virtual Worlds*, vol. 32, no. 1, e1970, 2021, ISSN: 1546-427X. DOI: 10.1002/cav.1970. [Online]. Available: https://onlinelibrary.wiley.com/doi/abs/10.1002/cav.1970.

[85] H. Sigurdsson, S. Carey, M. Alexandri, *et al.*, "Marine investigations of Greece's Santorini Volcanic Field", *Eos, Transactions American Geophysical Union*, vol. 87, no. 34, p. 337, 2006, ISSN: 0096-3941. DOI: 10.1029/2006EO340001. [Online]. Available: http://doi.wiley.com/10.1029/2006EO340001.

[86] A. L. Rizzo, A. Caracausi, V. Chavagnac, *et al.*, "Kolumbo submarine volcano (Greece): An active window into the Aegean subduction system", *Scientific Reports*, vol. 6, p. 28 013, Jun. 17, 2016, ISSN: 2045-2322. DOI: 10.1038/srep28013. pmid: 27311383.

[87] Paraskevi Polymenakou, director, *Submarine Kolumbo volcano, Santorini volcanic field, Greece (HCMR)*, Nov. 1, 2013. [Online]. Available: https://www.youtube.com/watch?v=9lI6FDNm5Qg.

[88] I. M. Dart, G. De Rossi, and J. Togelius, "SpeedRock: Procedural rocks through grammars and evolution", in *Proceedings of the 2nd International Workshop on Procedural Content Generation in Games*, Bordeaux France: ACM, Jun. 28, 2011, pp. 1–4, ISBN: 978-1-4503-0872-4. DOI: 10.1145/2000919.2000927. [Online]. Available: https://dl.acm.org/doi/10.1145/2000919.2000927.

[89] Epic Games, *Unreal Engine*, version 4.27. [Online]. Available: https://www.unrealengine.com/.

[90] SideFX, *Houdini*, version 20.0. [Online]. Available: https://www.sidefx.com/products/houdini/.

[91] Erwin Coumans and Yunfei Bai, *PyBullet, a Python module for physics simulation for games, robotics and machine learning*, version 3.2.5. [Online]. Available: http://pybullet.org.